

The discovery of low-mass pre main sequence stars in Cepheus OB3b

M. Pozzo^{1,3}, T. Naylor^{2,3*}, R.D. Jeffries³, J.E. Drew¹

¹ Imperial College London, Blackett Laboratory, Prince Consort Road, London, SW7 2BW, U.K.

² School of Physics, University of Exeter, Stocker Road, Exeter, EX4 4QL, U.K.

³ Astrophysics Group, School of Chemistry and Physics, Keele University, Staffordshire, ST5 5BG, U.K.

ABSTRACT

We report the discovery of a low-mass pre-main-sequence (PMS) stellar population in the younger subgroup of the Cepheus OB3 association, Cep OB3b, using *UBVI* CCD photometry and follow-up spectroscopy. The optical survey covers about 1300 square arcmin on the sky and gives a global photometric and astrometric catalogue for more than 7000 objects. The location of a PMS is well defined in a V versus (V-I) colour-magnitude diagram (CMD).

Multi-fibre spectroscopic results for optically-selected PMS candidates confirm the T Tauri nature for 10 objects, with equal numbers of classical TTS (CTTS) and weak-line TTS (WTTS). There are 6 other objects which we classify as possible PMS stars. The newly discovered TTS stars have masses in the range $\sim 0.9 - 3.0 M_{\odot}$ and ages from < 1 to nearly 10 Myr, based on the Siess, Dufour & Forestini (2000) isochrones. Their location close to the O and B stars of the association (especially the O7n star) demonstrates that low-mass star formation is indeed possible in such an apparently hostile environment dominated by early-type stars and that the latter must have been less effective in eroding the circumstellar discs of their lower mass siblings compared to other OB associations (e.g., λ Ori). We attribute this to the nature of the local environment, speculating that the bulk of molecular material, which shielded low-mass stars from the ionising radiation of their early-type siblings, has only recently been removed.

Key words: open clusters and associations: individual: Cepheus OB3 - stars: pre-main-sequence - stars: formation - stars: low-mass, brown dwarfs - accretion, accretion discs - techniques: radial velocities - techniques: spectroscopic

1 INTRODUCTION

In the last few years it has become increasingly recognised that the majority of low-mass stars in the solar neighbourhood are likely to have formed in OB associations. From extinct radionuclide abundances, it also seems plausible that our Sun was born close to an OB association (see Harper 1996, and references therein). OB associations are therefore key to understanding star formation processes and testing the universality of the initial mass function (IMF). From recent studies, the number of low-mass stars formed seems to follow the Miller-Scalo IMF of the field stars (see for example Walter & Boyd 1991; Walter et al. 1994; Preibisch & Zinnecker 1999; Preibisch, Guenther & Zinnecker 2001; Dolan & Mathieu 2001).

Although OB associations are by definition unbound, they are young enough that dynamical effects such as mass

segregation and preferential evaporation of lower mass stars (de la Fuente Marcos 1995) will not have occurred. It is crucial to establish the influence that high-mass neighbours have on the formation and evolution of their lower mass siblings. The winds and ionising radiation of hot stars could influence the mass function and circumstellar disc lifetimes of the lower mass stars, with implications for angular momentum evolution and planet formation. These ideas have gained currency with the discovery of evaporating discs around PMS stars in the Orion nebula (McCaughrean & O’Dell 1996) and theoretical studies showing that discs could be ionised and evaporated by the UV radiation fields of O stars (Johnstone, Hollenbach & Bally 1998).

The fact that the majority of low-mass stars are likely to form in high-mass OB associations has not inspired a huge number of observational projects to look for them, because of their faintness and the large association dimensions. Objective-prism H α studies were the first tool used to identify young low-mass PMS stars. These were mainly classical

* Guest investigator of the UK Astronomical Data Centre.

T Tauri stars (CTTS) which show the strongest $H\alpha$ emission (see reviews by Herbig 1962; Bastian et al. 1983; Bertout 1989; Appenzeller & Mundt 1989). These studies were followed by X-ray surveys, which have proved to be a convenient method to find mainly the more weakly $H\alpha$ emitting, so-called weak-line T Tauri stars (WTTS; see discussion in Stelzer & Neuhäuser 2001): these seem to be stronger soft X-ray emitters than CTTS, perhaps because of their faster rotation (see Bouvier et al. 1993, 1995; Wichmann et al. 1998) or perhaps because a large fraction of the X-ray flux is likely to be absorbed by the optically thick circumstellar material around CTTS (see Gahm 1981; Walter & Kuhi 1981; Flaccomio, Micela & Sciortino 2003a). Besides such a bias against CTTS, there is also a more general possible incompleteness problem: Wolk (1996) found X-ray selected PMS stars sharing the same position in the CMD of non X-ray selected PMS stars – demonstrating the presence of less magnetically active PMS stars. Recent surveys by more sensitive X-ray satellites such as *Chandra* and *XMM-Newton* can mitigate against both these biases, if such surveys are deep enough. For instance a very large fraction of optical and IR low-mass members of the Orion nebula cluster were detected as *Chandra* X-ray sources (Feigelson et al. 2002; Flaccomio et al. 2003b).

With the advent of larger-area sensitive detectors, it has become possible to undertake photometric studies of OB associations covering large areas with CCD mosaics, yielding identifications of the faintest low-mass members (e.g., Pozzo et al. 2000). When coupled with follow-up spectroscopy (e.g., Dolan & Mathieu 1999, 2001; Rebull et al. 2000; Preibisch et al. 2001) these surveys can overcome any possible biases associated with X-ray selected samples (Walter et al. 2000). This is the method we used for the investigation of our target region, the Cepheus OB3 association.

Cepheus OB3 is a very young association at about 800 pc from the Sun (Moreno-Corral et al. 1993), with galactic coordinates $l^{II} = 109.3^\circ - 111.7^\circ$ and $b^{II} = 2.4^\circ - 3.7^\circ$ (Blaauw 1964). It covers a region on the sky from about $22^h 46^m$ to $23^h 10^m$ in right ascension, and from about $+61^\circ$ to $+64^\circ$ in declination. It is composed of two main subgroups: the older, Cep OB3a, whose largest projected dimension is 17 pc; and the younger, Cep OB3b (shown in the Palomar Sky Survey image in Fig. 1), more compact and closer to the molecular cloud, whose largest projected dimension is 10 pc (Blaauw 1964).

Blaauw, Hiltner & Johnson (1959, and *erratum* in 1960; hereafter BHJ) identified 40 association members in total, comprising three late O-type and 33 B-type stars; some PMS members were proposed by Garmany (1973) and Sargent (1979); 8 new association members were recently proposed by Jordi, Trullols & Galadi-Enr iquez (1996; hereafter J96).

The ages of Cep OB3a and Cep OB3b were estimated by isochrone fitting to the high-mass stars to be about 10 ± 2 Myr and 7 ± 2 Myr respectively (see Blaauw 1964, 1991; de Zeeuw & Brand 1985). Ages derived from such isochrone fitting must be treated with caution in young OB associations: a better way is to look for low-mass stars which are still contracting towards the main-sequence. Note, however, that masses and ages remain model dependent. As a consequence, the shape of both the evolutionary tracks and of the isochrones change from one model to another, leading to discrepancies in the age estimates.

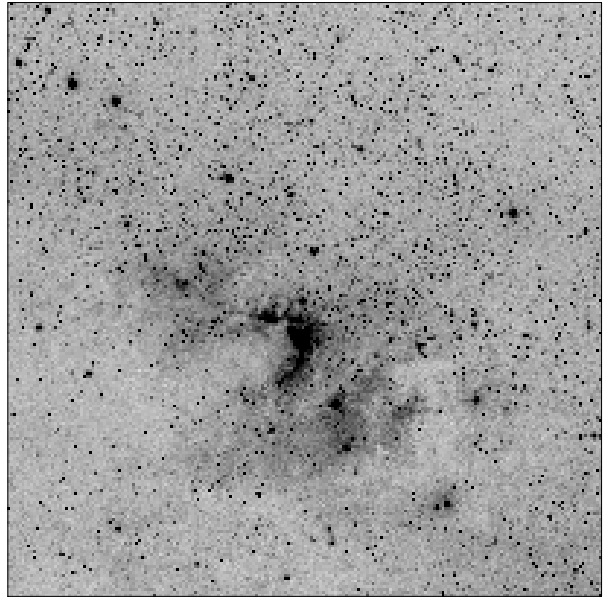


Figure 1. The Palomar Sky Survey image ($\sim 1.7^\circ \times 1.7^\circ$) of the region surrounding the Cep OB3b subgroup.

Much lower values of $\simeq 0.5$ Myr can be found in the literature for ages derived using the expansion age (kinematic methods) of the two Cep OB3 subgroups separately, or the association as a whole (De Veigt 1966; Garmany 1973; Assousa, Herbst & Turner 1977; Sargent 1979; Trullols et al. 1997). Compared with the much larger nuclear ages from isochrone fitting there is an apparent paradox. However, the kinematic methods have been shown most commonly to underestimate the true age (i.e., the nuclear age; Brown, Dekker & de Zeeuw 1997). Brown et al. (1997) advise that a kinematic age of ~ 0.5 Myr for Cep OB3 “should be treated with caution”.

What was the trigger which initiated star formation in Cep OB3 (i.e. the older subgroup Cep OB3a)? And what was subsequently responsible for the creation of the younger subgroup Cep OB3b? Are there signs of further star formation processes indicative of a third generation of newly born stars in the association? The members of the younger subgroup lie between the older subgroup and the molecular cloud. In the darkest part of the cloud, $A_V = 46$ (Felli et al. 1978), and so any optical detection of embedded stars is impossible. The fact that there is a temporal separation between the older and the younger subgroup of about 3 Myr as well as a spatial separation of about 13 pc strengthened the hypothesis of the sequential model (Elmegreen & Lada 1977) for star formation in the Cep OB3 association (see Sargent 1979). According to this model, the ionising radiation of early-type stars is responsible for the propagation of a shock wave front through the cloud, making the material gravitationally unstable and causing its condensation into new massive stars. In other words, once a subgroup is formed, another one grows thanks to shocks driven by the previous one.

A different scenario was instead proposed by Assousa et al. (1977), who confirmed the existence of an H I expanding

shell around Cep OB3, first discovered by Simonson & van Someren Greve (1976) from 21-cm radio line observations. The H I shell was found to be centred on the older subgroup (NE of the younger subgroup), with a radius of about 53 pc and expanding with a velocity of 35 km s^{-1} . The shell was identified with a supernova (SN) remnant (type II) of age 0.43 Myr. The pulsar PSR 2223+65, 1.14 Myr old, was suggested as a possible stellar remnant of the SN event. In light of these results, Assousa et al. (1977) proposed a SN-induced star formation process for the younger subgroup, Cep OB3b, which was then estimated to be of age 0.3 Myr by kinematic methods. We know now that Cep OB3b is instead likely to be a few Myr old, implying that the proposed pulsar is too young to be the remnant of the SN triggering star formation in this subgroup. However, another pulsar quoted by Assousa et al. (1977), PSR 2324+60, some 10 Myr old, may be a better candidate for having indeed triggered star formation not only in the younger subgroup but, possibly, in the older subgroup too.

Finally, the geography of the region must be considered in detail. The molecular cloud is in physical contact with the S155 H II region (see Panagia & Thum 1981), about 35 pc in size (Heyer, Carpenter & Ladd 1996), which was created by the ionising radiation of the OB stars. A bright arc of nebulosity defines the interface between the S155 H II region and the molecular cloud (see Fig. 1). The presence of an H II region and of a reflection nebula, i.e. the signs of the interaction between the molecular cloud and the OB stars previously formed in the association, confirm that recent star formation has taken place in the region. This is supported by the radio and near-infrared survey results of Testi et al. (1995), suggesting the presence of a cluster of young embedded stars which could represent the third generation of early-type stars in Cep OB3. Recently, Naylor & Fabian (1999) have discovered more than 50 X-ray sources in Cep OB3b thanks to *ROSAT* observations: their X-ray properties strongly suggest their likely T Tauri nature, corroborating the hypothesis that the presence of high-mass stars does not halt low-mass star formation, as previously widely thought. Furthermore, the discovery of another compact H II region, south of Cep OB3b (Harten, Thum & Felli 1981), picks out another possible area of active star formation. Given these results, we decided to investigate this long-studied association, concentrating our attention on the younger subgroup, Cep OB3b.

In this paper we present and discuss an *UBVI* CCD photometric study of the Cep OB3b subgroup. For the first time, thanks to the wide surveyed area (of about 1300 arcmin^2) and deep photometry, we have been able to unambiguously detect low-mass pre-main sequence members of the Cep OB3 association. An optically-selected sample of PMS candidates was spectroscopically followed-up at optical wavelengths, to test for kinematic membership of the association and confirm youth through radial velocity and Li I 6708 Å equivalent width measurements.

The paper is organised as follows. In Section 2, photometric observations and the data reduction are presented; colour-magnitude diagrams for each of the observed fields are described in Section 3. Section 4 deals with the investigation of the stars in the colour-magnitude diagrams by means of the *Q*-method and by cross-correlation of our optical photometric catalogue with the *ROSAT* X-ray selected

young star candidates presented by NF99. In Section 5 we discuss the results obtained from a spectroscopic follow-up of our photometry: using radial velocity measurements, spectral classification and Li I 6708 Å equivalent widths we identify PMS objects in Cep OB3b. Possible age gradients of PMS objects suggested by isochrone fitting are studied in Section 6. Discussion is presented in Section 7 and conclusions follow in Section 8.

2 OPTICAL PHOTOMETRIC OBSERVATIONS AND DATA REDUCTION

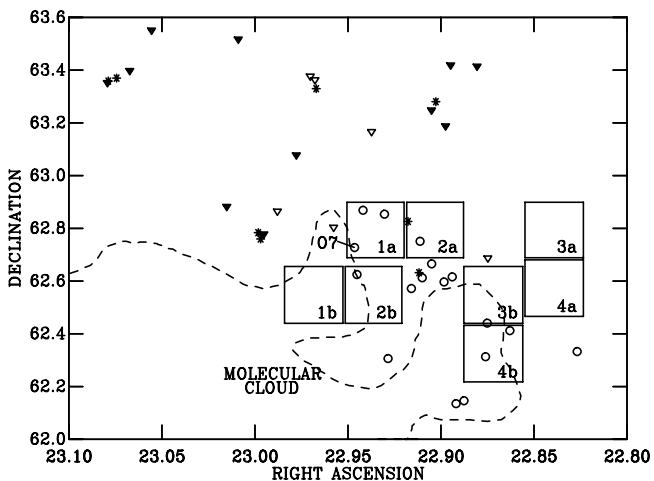
The *UBVI* CCD images were taken on the nights of August 10/11 and 11/12 1997, with the 2.5-m Isaac Newton Telescope (INT), La Palma, Canary Islands, Spain, equipped with the Wide Field Camera (WFC) and an array of 4 Loral CCDs. Data were taken using filters *U* (RGO), *B* (Harris), *V* (Harris) and *I* (RGO INT-WFC). Even though the WFC was composed of four Loral CCDs, only data from CCD2 and CCD4 were reduced: CCD1 was dead, while CCD3 had a sensitivity problem and a very non-uniform response. The images cover approximately $12 \times 12 \text{ arcmin}^2$ each (one pixel is equivalent to about 0.37 arcsec on the sky). Field centres and exposure times are listed in Table 1. Fig. 2 shows the surveyed region. The average seeing was 1.3 arcsec during the first night of observation, and 1.1 arcsec in the second night. Both nights were photometric.

After the images had been debiassed and flat fielded, we extracted the flux for each star in the field using the optimal extraction techniques outlined in Naylor (1998) and Naylor et al. (2002). Our final catalogue gives *V*, (*U*-*B*), (*B*-*V*) and (*V*-*I*) for each star along with an associated error and a flag. Non-zero flags are used to report problems with particular stars which make the data unreliable, details of which are given in Naylor et al. (2002). The catalogue also contains astrometric positions for each star, using a slightly modified version of the procedure described in Naylor et al. (2002). All of fields 1a, 2a and 2b, and 80 percent of 1b are covered by the second incremental release of the 2 Micron All-Sky Survey (2MASS) catalogue. So we began fitting our X-Y positions to the 2MASS positions, using a nine co-efficient model, which included the tangent point and a pincushion co-efficient as free parameters. The mean pincushion co-efficient was consistent with the nominal value of 220 rad^{-2} for the INT prime focus, so this was adopted for all the fields. We then re-fitted all the CCDs, this time using the (less accurate) USNO A-2.0 catalogue positions (Monet 1998) for the fields where 2MASS was not available, to derive the mean tangent point for each pointing by averaging the value for the two CCDs. This allowed a final six co-efficient model to be fitted, using (for consistency) USNO A-2.0 for all fields. The RMS residual about the fits was about 0.35 arcsec, though more in fields 4b and 1a (0.43 and 0.53 arcsec respectively) where there were a shortage of USNOA-2.0 stars.

As explained in Naylor et al. (2002), to derive the magnitudes in the catalogue, we need a set of photometric co-efficients derived using a relatively large aperture. To achieve this we observed one field in the older subgroup (termed the local field) at four different times during the run. We then measured bright stars in this field with varying size aper-

Table 1. CCD fields surveyed in the Cep OB3 region. Fields a correspond to CCD2, fields b to CCD4 (see Figure 2).

CCD fields	centre (RA, dec) (J2000.0)		Exposure times (sec) in U,B,V,I (long; short)			
1a	22 56 06.78	+62 47 31.67	100, 40, 20, 10;	10, 4, 1, 1		
1b	22 58 05.34	+62 32 41.21	100, 40, 20, 10;	10, 4, 1, 1		
2a	22 54 11.77	+62 47 42.84	100, 40, 20, 10;	10, 4, 2, 1		
2b	22 56 10.43	+62 32 52.44	100, 40, 20, 10;	10, 4, 2, 1		
3a	22 50 21.14	+62 47 44.88	100, 40, 20, 10;	10, 4, 2, 1		
3b	22 52 19.63	+62 32 53.92	100, 40, 20, 10;	10, 4, 2, 1		
4a	22 50 21.78	+62 34 22.50	100, 40, 20, 10;	10, 4, 1, 1		
4b	22 52 18.97	+62 19 32.20	100, 40, 20, 10;	10, 4, 1, 1		

**Figure 2.** Our surveyed region in the Cep OB3 association. The superimposed boxes are our survey CCD fields for CCD2 (fields a) and CCD4 (fields b). BHJ members of the Cep OB3a subgroup are shown as filled triangles, those of Cep OB3b as open circles; possible PMS stars from Garmany (1973) and Sargent (1977) are shown as open triangles; new possible members (J96) as asterisks; the O7n star (BHG 41) is marked; the dashes represent the lowest ^{12}C O contour of peak antenna temperatures for the molecular cloud (taken from Sargent 1977).

tures, and found that the smallest scatter between measurements was achieved using a radius of 15 pixels, or 5.6 arcsec. We then used this aperture to measure a total of 48 standard stars from three Landolt (1992) standard fields which were observed over both nights for both CCDs. To derive the photometric co-efficients from these measurements we assumed (i) the colour terms were the same on both nights, but were different for each CCD; (ii) the extinction coefficient was the same for both CCDs, but different on each night; and (iii) the zero points were different for the two CCDs and from night to night. This required a fit to 8 parameters, (i.e., 2 colour terms, 4 zero points and 2 extinction coefficients), for each colour transformation equation. The fit is based on a weighted least-squares method. A systematic error was added in quadrature to the total error in order to find a reduced χ^2 equal to 1. The additional systematic errors were about 1 per cent for the (V-I), (B-V) and V calibrations, but about 2.7 per cent for (U-B), as we expected, since the U-band is always most problematic for CCD observations. Multiple observations of the local field allowed us to test

our final field-to-field internal precision, which was about 0.02 mag.

We removed from the catalogue those stars for which no (V-I) colour or visual magnitude was determined to better than 0.1 mag and/or with corresponding non-zero flags. The resulting catalogue contained 7315 objects, with visual magnitudes in the range $12.32 \leq V \leq 21.04$ mag and colours in the range $0.02 \leq V - I \leq 6.58$ (on the Cousins system). This will be the only catalogue used in the subsequent analysis, unless otherwise specified. The photometry has uncertainties smaller than 0.1 mag in all the *UBVI* colours for 1241 objects, with visual magnitudes in the range $V = 12.32 - 19.88$ mag. Limiting magnitudes for each filter (corresponding to an error of 0.1 mag) are about $U = 22.4$, $B = 21.8$, $V = 21.0$ and $I = 20.0$.

For completeness, we have correlated our optical photometric catalogue with the much smaller one of Jordi et al. (1995) in Appendix A. We found evidence for only small systematic discrepancies.

3 COLOUR-MAGNITUDE DIAGRAMS

In Fig. 3, the colour-magnitude diagrams (CMDs) in V versus (V-I) for all the CCD fields are shown. Also plotted there is the mean reddening vector we have adopted for the Cep OB3b subgroup, with $\langle A_V \rangle = 2.81 \pm 0.10$ and $E(V - I) = 1.18 \pm 0.03$, derived from the relation $E(V - I) = 1.3 * E(B - V)$, taken from the reddening relationship of Winkler (1997), with $E(B - V) = 0.91 \pm 0.02$. These values, and the mean distance modulus ($dm = 9.65 \pm 0.20$ mag, corresponding to a distance of about 850 ± 80 pc) were determined from data given by Moreno-Corral et al. (1993). They derived the extinction law for each of 14 OB stars individually, obtaining a mean $R (= A_V / E(B - V))$ value of 3.1 ± 0.1 . The A_V values for these stars range from 2.37 to 4.27 mag, while R ranges from 2.44 to 3.61. We omitted BHJ 11 from the mean reddening determination because its membership is doubtful, due to its position on the H-R diagram and its extinction, $A_V = 4.3$, which both differ from those of the confirmed Cep OB3 members (see Sargent 1979). However, we point out that its inclusion in the calculation would have had little effect, the slope of the reddening vector staying practically the same in the CMDs.

Even though $R < 3.6$ for the early-type stars, it is possible that these are not entirely representative of the whole Cep OB3b region: given that the majority of the members are still close to, or embedded, in the molecular cloud, it would not be surprising if R were larger for some fraction of the subgroup members. Indeed, it has been shown that R can be as high as 5 in the neighbourhood of star forming regions (Mathis 1990). In other words, we do not necessarily expect R to have an homogeneous value across the younger subgroup. A larger R value would steepen the inclination of the reddening vector in the CMDs. For $R \approx 5$ and our preferred $A_V = 2.81$, $E(V - I)$ would decrease by ~ 0.2 . In our later comparison of isochrones, reddened according to the adopted mean extinction (see Section 6), stars with an R value higher than the adopted 3.1 will in fact be younger than they appear.

Fig. 4 shows the location of the Cep OB3b members, with their associated BHJ numbers: the stars which were

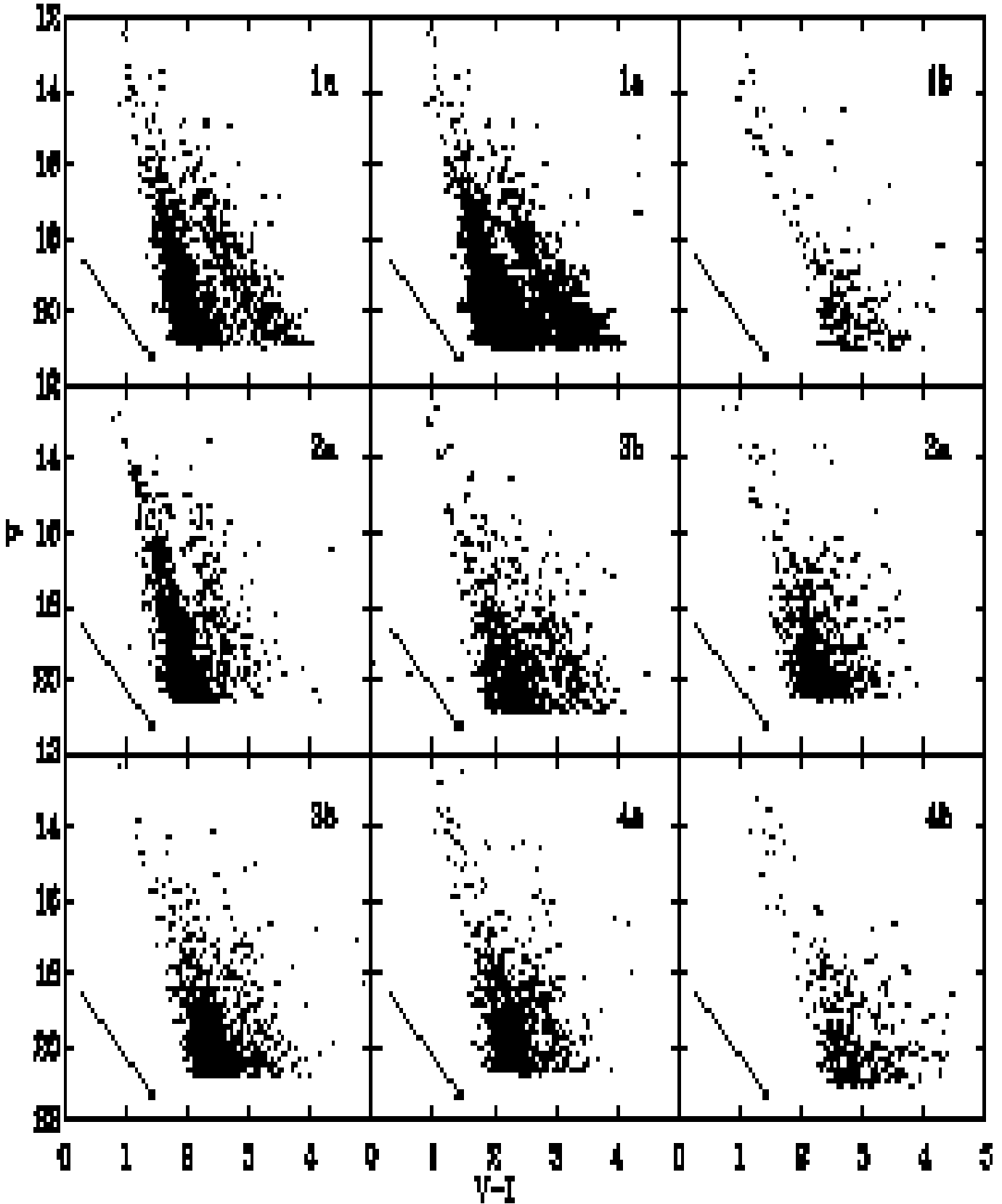


Figure 3. Colour-magnitude diagrams in V versus (V-I) for the surveyed fields as labelled. The average reddening vector for Cep OB3b is shown, with $\langle A_V \rangle = 2.81$ and $E(V - I) = 1.18$ (see Section 3). Also plotted (top-centre) there are error bars for the field 1a data points (error bars for $V = 12, 17, 20$ are shown as reference).

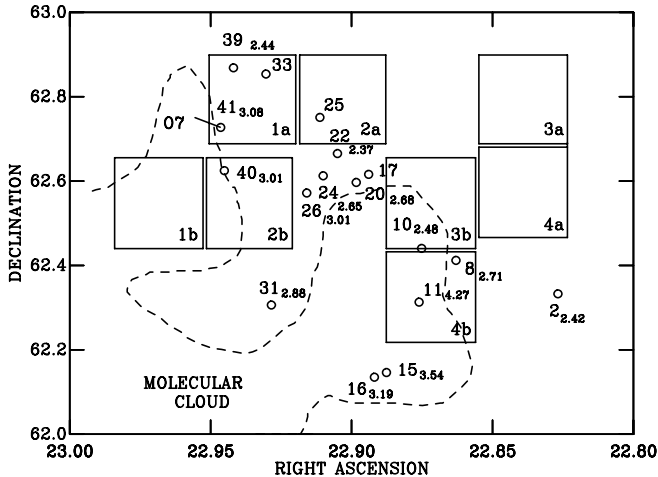


Figure 4. The Cep OB3b subgroup, with known members shown as circles and their corresponding BJJ number (other symbols as in Fig. 2). Those objects used to determine the mean reddening value have also a subscript indicating their A_V value given by Moreno-Corral et al. (1993). The A_V value for BJJ 11 is also given, although not used in our calculation.

used by us for the determination of the mean reddening value have their A_V value as subscript (we give this value for BJJ 11 too, although not used in the calculation).

4 WHAT ARE THE STARS IN THE COLOUR MAGNITUDE DIAGRAMS?

4.1 Q -method: the background population

Let us analyse the CMDs in V versus $(V-I)$ shown in Fig. 3, obtained for each of the 8 CCD fields, in order to begin to identify the stars within them.

The first thing which catches the eye is that in the CMDs of fields 1a, 2a and 2b (see Fig. 3) there are two clear sequences. The bluer of the two is the more densely populated in all three fields. By contrast, in the CMD of field 1b (see Fig. 3, top-right) most of this bluer sequence is missing. Field 1b is directly towards the molecular cloud where we would expect to see mainly foreground stars and slightly reddened stars associated with it. We therefore conclude that the blue sequences observed off-cloud in fields 1a, 2a and 2b are due to a background population. The separation of the redder sequences from these blue sequences is not the product of random errors in the photometry. As an example illustrating this, the plot given in Fig. 3, top-centre, shows the data for field 1a with associated error-bars. We cannot identify any likely systematic error in the photometry that could have led to an artificial division of the stars into two sequences.

To gain an impression of the distance to the background objects we consider field 1a, where the separation of the two sequences is particularly clear. A first guess can be made if we plot the number of stars as a function of the distance modulus $dm (= V - M_V - A_V = 5 \log d - 5)$. To do this we exploit the Q -method (Johnson & Morgan, 1953) which can uniquely find possible main-sequence members earlier

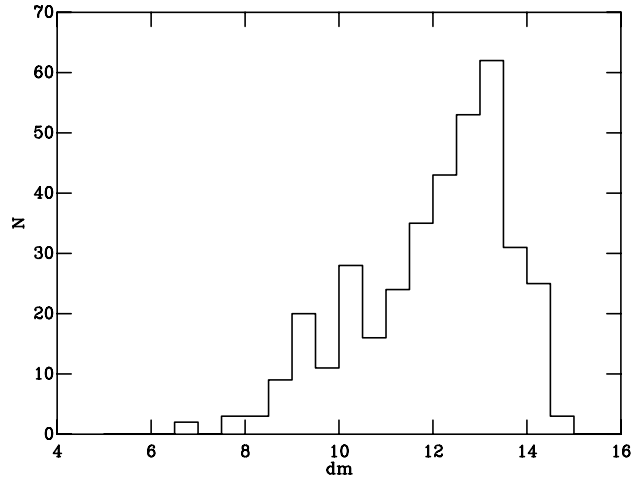


Figure 5. Number of stars per dm : the peak for Cep OB3b should be at about 9.6 mag. The considerable peaks at larger distance moduli show the presence of background populations.

than A5 (with luminosity classes III and V). This is because for these stars there is a unique *reddening independent* parameter $Q = (U - B) - 0.72 * (B - V)$, which is less than 0.47 for spectral types earlier than A5. Q permits us to determine the intrinsic $(B - V)$, according to the relation $(B - V)_0 = -0.009 + 0.337 * Q$. From intrinsic and measured $(B - V)$ colours we can then determine the colour excess $E(B - V)$ and therefore A_V according to the relation $A_V = R * E(B - V)$ (assuming $R = 3.1$). The absolute visual magnitude M_V , and hence $dm = V - M_V - A_V$, can then be found using a standard $M_V - (B - V)_0$ relation. We used the absolute-magnitude versus intrinsic $(B - V)$ calibration for the ZAMS stars given by Walker (1985).

We plot in Fig. 5 the distance modulus for all the stars in field 1a with Q values < 0.47 . Consistent with the Q limit, only intrinsic $(B - V)$ values in the range -0.32 to 0.15 are retained (see also Fitzgerald 1970). The great majority of the stars included in the histogram lie in the top part of the blue sequence seen in the V vs $(V-I)$ diagram. Stars belonging to Cep OB3b should have $dm \sim 9.65$ mag. As we can see from the plot, the distribution only just begins at this distance modulus and stretches to much larger values, with the mode at $13.0 < dm < 13.5$ mag, implying a distance range from 1 to 10 kpc. It seems reasonable to interpret these objects belonging to the blue sequence as mainly B stars (since A stars are more common but fainter), concentrated in spiral arms and less than 100 Myr old. There seem to be only a few objects associated with the Cep OB3b subgroup at ~ 800 pc.

It is known that Cep OB3 is in the Cygnus-Orion arm, between the Sagittarius-Carina arm and the Perseus arm. According to Verschuur (1973), the latter extends in distance from about 2.5 to 4.0 kpc (corresponding to a reddening-free distance modulus of between 12 and 13 mag). There is also evidence for the existence of a second arm beyond the Perseus arm extending to higher galactic latitudes, passing through the line of sight of Cep OB3b (Kimeswenger & Weinberger 1989; Ungerechts, Umbanhowar & Thaddeus 2000). In addition, Wouterloot et al. (1990) combined CO

Table 2. Optical counterparts to the *ROSAT* X-ray sources of NF99. The listed coordinates are from our optical photometric catalogue.

X-ray id. ^a	V (NF99)	n.c.	sep. (arcsec)	Field	RA (J2000)	Dec (J2000)	V	(V-I)
14 (P)		6	7.1	1a	22 55 30.103	+62 47 39.56	16.94	2.18
20 (P)		1	7.5	1a	22 56 01.546	+62 47 47.12	17.94	2.74
24 (H)		7	3.2	1a	22 56 18.345	+62 45 16.84	18.14	2.80
26 (P)		7	3.8	1a	22 56 20.132	+62 52 23.16	16.79	2.44
27 (H)	15.3	10	4.8	1a	22 56 26.417	+62 41 29.23	15.38	1.91
29 (P)	15.5	6	7.4	1a	22 56 29.678	+62 45 28.68	15.66	1.96
34 (H)	14.2	5	1.6	2b	22 56 38.721	+62 37 14.43	14.55	2.26
35 (H)	14.9	7	3.7	1a	22 56 39.087	+62 45 09.36	14.91	1.89
44 (P)	13.5 (GSC)	3	6.0	1a	22 56 56.417	+62 52 42.45	14.36	1.48 ^b
48 (P)		2	12.9	2b	22 57 05.220	+62 38 38.60	15.15	1.51

^a (P) is for PSPC, (H) for HRI.

^b This object is very close (8 pixels, corresponding to 2.96 arcsec on the sky) to another star not numbered in the catalogue: possible binary?

Table 3. Probability of finding a correlation (the brightest) with a shifted PSPC (P) and HRI (H) X-ray source and the expected number of spurious correlations as a function of V.

range	Prob(P)	Prob(H)	N(P) ^a	N(H)	N _r (P) ^b	N _r (H)
V < 15.15	0.02	0.02	1	2	0	0
V < 16.15	0.05	0.02	3	3	0	0
V < 17.15	0.06	0.04	5	3	0	0
V < 18.15	0.10	0.09	6	4	1	0

^a The number of correlations with the original X-ray sources in the V range shown.

^b The number of random correlations expected in the V range shown.

measurements with IRAS point source data to show that star formation is indeed occurring along the Cep OB3b sight-line out to ~10 kpc (see their figure 4). Fig. 5 confirms that there is a considerable assemblage of stars beyond Cep OB3b.

This same background population is apparent as the blue sequence in each of fields 2a and 2b. We have already noted that this sequence is essentially absent from field 1b, positioned directly on the molecular cloud. In fields 3a, 3b and 4a (see Fig. 3), the background population of stars is still apparent but there is not the neat separation between it and the redder population. This is presumably because the background objects are shifted towards larger (V-I) colours due to additional interstellar material in these directions (see Appendix B). Field 4b (see Fig. 3, bottom-right) is transitional in character between these fields and the on-cloud 1b field.

4.2 Cross-correlation with X-ray sources: hints of a pre-main sequence population

We cross-correlated our optical catalogue with the (0.1-2.4 KeV) *ROSAT* X-ray sources recently detected by Naylor & Fabian (1999; hereafter NF99). The suggestion made by NF99, that these X-ray sources are T Tauri stars (low-mass PMS stars are strong X-ray emitters; see for example Feigelson & DeCampli 1981; Strom et al. 1990; Wichmann et al. 1997; Feigelson & Montmerle 1999), is strongly supported by both the ratio of X-ray to optical luminosity for the faintest objects of about $10^{-1.5}$ (which is typical of very active stars; see Stocke et al. 1983), and by their X-ray variability, with values typical of other PMS associations (see Montmerle et al. 1983). 30 of the NF99 sources fall within our CCD fields.

We determined the separations between the X-ray sources and possible optical counterparts, and accepted correlations within 15 arcsec of Position Sensitive Proportional Counter (PSPC) positions, and 7 arcsec of the more accurate High Resolution Imager (HRI) positions. There were 8 X-ray sources with no optical counterparts within these errors circles. When more than one optical counterpart was found, the brightest was then chosen because X-ray luminosity is approximately proportional to the optical luminosity (see Feigelson et al. 1993). At this stage, 12 more of the X-ray sources had to be dropped from the sample because their optical counterparts suffered photometric problems or errors in colours larger than the 0.1 mag acceptance limit. This left a total of 10 counterparts to the NF99 X-ray sources with good photometry, as listed in Table 2. X-ray source number

and visual magnitude from NF99 are given respectively in columns 1 and 2. The number of correlations with optical counterparts within our adopted error circles is given in column 3. Column 4 refers to the separation to the brightest optical counterpart belonging to the field specified in column 5 (as given in Fig. 2). Columns 6 - 9 list the positions, visual magnitudes and (V-I) colours of the brightest optical counterparts.

We also derived the number of random correlations to be expected among those found. For this purpose, we repeated the cross-correlation by shifting the X-ray positions of NF99 by 20 arcsec north, south, west and east, and retaining only acceptable correlations according to the criteria used before. The probability of having a correlation with one of the shifted X-ray sources in a specified V range is reported in Table 3, for the PSPC and HRI respectively (columns 1-3). Also tabulated are the number of good correlations found with the original X-ray sources (columns 4-5) and the number of random correlations (columns 6-7) in the corresponding V range for PSPC and HRI respectively. We therefore expect at most one out of the 10 optical counterparts to be a random correlation (more precisely, one out of the 6 which are correlated with a PSPC X-ray source).

We stress that although there are several (up to 10) optical correlations within our adopted X-ray error circles, the vast majority of these are very faint, not candidate PMS members of Cep OB3b and not credible candidate active stars (their X-ray to optical flux ratio would be much too large). Furthermore, the "spurious" correlation probabilities we show are for the entire CMD. Spurious correlations are most likely to be found at colours where the stellar density is highest for each V range and so not near the putative Cep OB3b PMS we describe below. The density of candidate PMS stars is not large enough to make it likely that more than one such star contributes to each X-ray source. Lastly, the spurious correlation probabilities were calculated using a 7 and 15 arcsec X-ray error circle for the HRI and PSPC sources respectively. All but one of the correlations (one of the optically brightest – see below) are within the central 50 per cent of their respective X-ray error circles, reducing the likelihood of them being random correlations by a further factor of two over the figures quoted in Table 3. Whilst we are thus quite confident that the optical counterparts we have selected are indeed X-ray sources, we anticipate that the scheduled *Chandra* AO-4 observation of Cep OB3b (P.I. G. Garmire) will add a great deal, both in terms of its greater sensitivity – enabling the detection of many fainter, less magnetically active PMS stars, and with its narrower point spread function – allowing unambiguous optical counterpart identification.

Fig. 6 shows the location of the 10 optical counterparts to the X-ray sources of NF99 with respect to the CCD fields. All but two of them belong to field 1a, and lie in the redder sequence of the CMD shown in Fig. 7. This is consistent with the idea, but it does not yet prove, that this sequence is a PMS, including young, active stars. There is still the possibility of contaminating foreground and background X-ray active stars. Note that the optical counterpart to one of the X-ray sources (no. 48) in field 2b is the one closest to the "background" sequence in Fig. 7, at $V=15.15$ and $(V-I)=1.51$ and the most widely separated counterpart from its X-ray source. According to the results of our spectroscopic

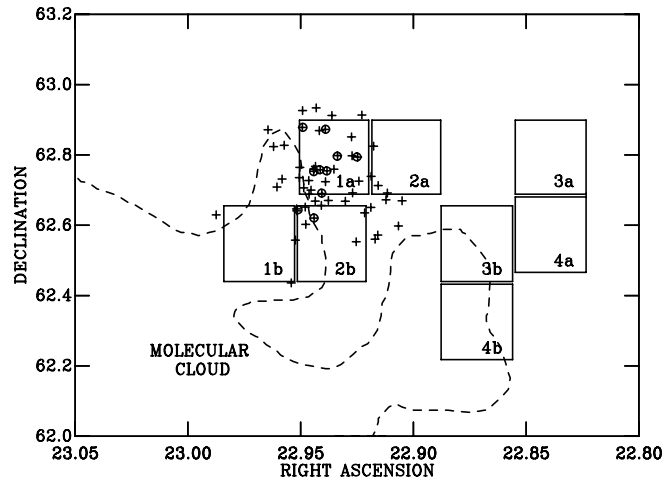


Figure 6. The location of the 10 optical counterparts (circled) to the X-ray sources of NF99 listed in Table 2. X-ray sources of NF99 for which we do not have an optical counterpart are simply shown as crosses.

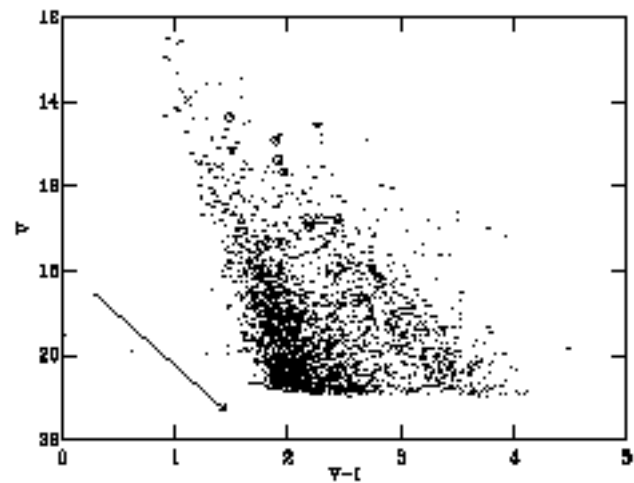


Figure 7. The CMD for fields 1a and 2b plotted together with the 10 optical counterparts to the X-ray sources of NF99: those falling in the field 1a are shown as circles, whereas the two on field 2b are shown as open triangles. Also plotted there is the average reddening vector for Cep OB3b, with $\langle A_V \rangle = 2.81$ mag and $E(V-I) = 1.18$ mag (see Section 3).

follow-up (see Section 5), it is an F-type star that cannot belong to Cep OB3b on the grounds of its radial velocity. This illustrates the essential role for spectroscopy, which we now turn to, in finally establishing the status of those stars belonging to the redder sequence in the CMDs.

5 SPECTROSCOPIC FOLLOW-UP

5.1 Selection of PMS candidates

Spectroscopic observations of the PMS objects found from our optical photometric survey are necessary to check their

nature, i.e. to test their kinematic membership of the association and confirm that they are truly young objects. The first objective is achieved with radial velocity measurements and the second can be achieved for cool stars by using the equivalent width of the Li I 6708 Å line as a youth discriminator (see Martín 1997).

During the PMS phase, fully convective low-mass stars contract and their cores heat up to the point at which Li can be burned in p,α reactions. Convective mixing ensures that photospheric Li is then also depleted on very short timescales. In more massive stars, photospheric Li depletion occurs when and if the base of the convection zone achieves the threshold temperature for Li burning. Thus a Li abundance close to that of the pristine interstellar medium is a signature of youth in stars of low and intermediate masses. Unfortunately, both the time dependence of Li depletion and observational practicalities mean that the sensitivity of the test is dependent on the spectral type of the star. Li is depleted very rapidly on timescales of a few Myr in stars of type late K and M. This timescale rises to 100 Myr for early K stars and perhaps to 1 Gyr for F stars (see Soderblom et al. 1993). At the same time, the strength of the Li 6708 Å resonance line, which is the only realistic diagnostic of Li abundance in stellar photospheres, declines drastically with increasing temperature. Thus, while the presence of undepleted Li is a necessary condition for F or G stars to be identified as PMS, it is not sufficient. For K and M stars the presence of undepleted Li is almost a guarantee of a PMS status. In practice this means we must identify a threshold EW for the Li 6708 Å line that is consistent with an undepleted Li abundance (see Section 5.4).

The objects for the spectroscopic follow-up observations were selected from the combined V versus (V-I) CMD for fields 1a, 2a, 3a, 4a, 2b, and 3b. Fields 1b and 4b were excluded because they are pointing at the molecular cloud, and are therefore most likely to contain only foreground objects. Had we wished to maximise the number of PMS stars in our spectroscopic sample we would have chosen a region which fitted tightly around the suspected (X-ray selected) PMS objects. However, since our aim was to find the limits of the PMS in V vs (V-I), we actually chose a region which encompasses the whole “second sequence” and also the red side of the “background” sequence. This sample should have little bias in terms of age and allow for differential reddening across the Cep OB3b subgroup (see Fig. 8).

All the catalogue stars with good flags and photometric errors less than 0.1 mag for V and (V-I), falling in the strip, were retained. An exception was made for those flagged as non-stellar objects, which were retained since they could be double stars. We did not select stars fainter than $V = 19$ mag, mainly because they would be too faint for spectroscopy. The result of this selection is shown in Fig. 8: selected objects are within the dashed box, optical counterparts to the *ROSAT* X-ray sources are circled. There are 1225 selected objects out of 7884.

We then performed a further selection by choosing stars having an error less than 0.1 mag and a good flag in the (B-V) colour too, and picking up only those stars which were contained in a strip in the (B-V) versus (V-I) colour-colour diagram, again defined by the optical counterparts to the *ROSAT* X-ray sources of NF99 (see Fig. 9). The result of this additional selection left 616 possible PMS objects.

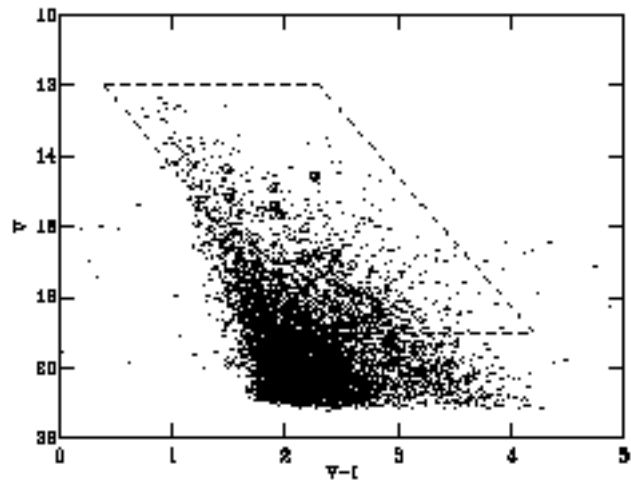


Figure 8. The PMS objects selected from the PMS strip (within the dashed box), encompassing the optical counterparts to the *ROSAT* X-ray sources of NF99 (circled).

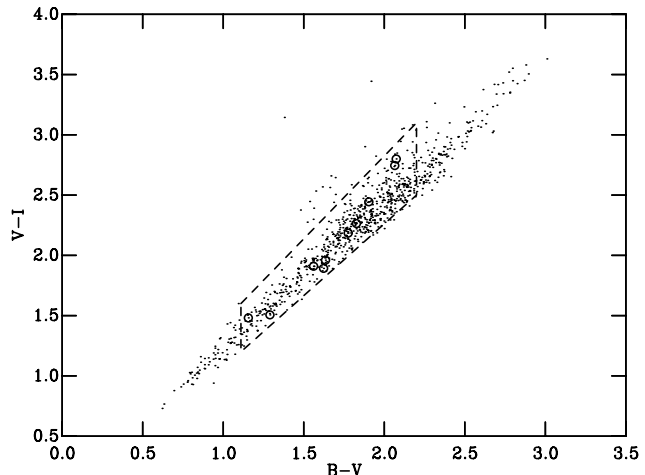


Figure 9. Additional selection from the possible PMS objects selected in the V versus (V-I) colour-magnitude diagram of Fig. 8. The resulting objects are contained in the dashed box, the optical counterparts to the *ROSAT* X-ray sources of NF99 are circled.

These objects were the initial sample for the spectroscopic investigation which was carried out with the multi-fibre spectrograph WYFFOS. The configuration program available for WYFFOS observations gave us two fields for a total of 110 (out of 616) optically-selected possible PMS objects.

5.2 WYFFOS/AF2

Intermediate-resolution spectra of the 110 optically-selected possible PMS objects were obtained on December 11-12, 1999, with the WYFFOS/AF2 multi-fibre spectrograph at the 4.2-m William Herschel Telescope (WHT), La Palma, Canary Islands, equipped with a CCD TEK 6 chip (type TK1024), the WYFFOS echelle grating (632 grating rulings/mm) and the echelle order-sorting filter number 4 (6625

Å) to cover the region occupied by the H α (6563 Å) and Li I (6707.8 Å) features.

We obtained a wavelength coverage of about 440 Å, in the approximate range 6380-6820 Å. The nominal dispersion is 17.8 Å/mm (equivalent to 0.43 Å/pixel), with a spectral resolution (FWHM) of about 2 pixels, equivalent to about 1 Å, determined from arc lines. Each fibre covers 2.7 arcsec in diameter on the sky.

Target, bias, arc, flat and offset sky frames were taken. Target frames were observed for 3×1800 s in the first configuration (first night), and for 3×1500 s in the second configuration (second night). Three offset sky frames (of 400s and 300s on the first and second nights respectively), were taken for each configuration by beam-switching the telescope to nearby sky (at 15 arcsec north, south and west of the target position). These were taken in order to normalise the fibre transmissions (throughput/vignetting correction), under the assumption that the night sky has the same brightness through each fibre. About 15 dedicated sky fibres were assigned in each configuration and these were used to determine the mean sky spectrum. In addition, we used the offset exposures to create a sky spectrum for each fibre (which was a mean of the offset sky exposures through that fibre). Sky subtraction using the offset sky exposures was used to create the spectra from which H α equivalent widths (EWs) were measured, since this minimised the effects of nebular contamination of the H α lines in target regions of high nebularity. The mean sky determined from dedicated sky fibres was instead used to create the spectra which were cross-correlated and from which Li I EWs were measured, since this resulted in higher signal-to-noise spectra. In addition, on the second night we measured some radial velocity standard stars through a single fibre at the centre of the field.

The IRAF[†] WYFRED procedures (Pollacco et al. 2000) were used to process the images and extract the multi-fibre spectra obtained with WYFFOS. From the residuals to continuum fits in line-free regions of the spectra, we derive a typical signal-to-noise of $S/N > 10$ for the majority of the targets.

5.3 Radial velocities

Radial velocity (RV) measurements were performed using the Starlink software package FIGARO. The spectrum of the IAU radial velocity standard star HD 213947 (spectral type K4 III) was extracted too. All the objects and standard spectra were re-binned to a logarithmic wavelength scale, giving constant velocity bins of 19.152 km s^{-1} . The targets were cross-correlated with the radial velocity standard star in the spectral range 6400-6550 Å (a region containing easily identifiable metallic lines), in order to determine the relative shifts, and calculate RVs. We also tried the region 6650-6800 Å but the cross-correlation peak was weaker and did not improve the result. Note that possible cosmic rays and N II ($\lambda\lambda$ 6548, 6584) or S II ($\lambda\lambda$ 6717, 6731) nebular emission lines

[†] IRAF (Image Reduction and Analysis Facility) is distributed by the National Optical Astronomy Observatory (NOAO), which is operated by the Association of Universities for Research in Astronomy (AURA), Inc. under cooperative agreement with the National Science Foundation.

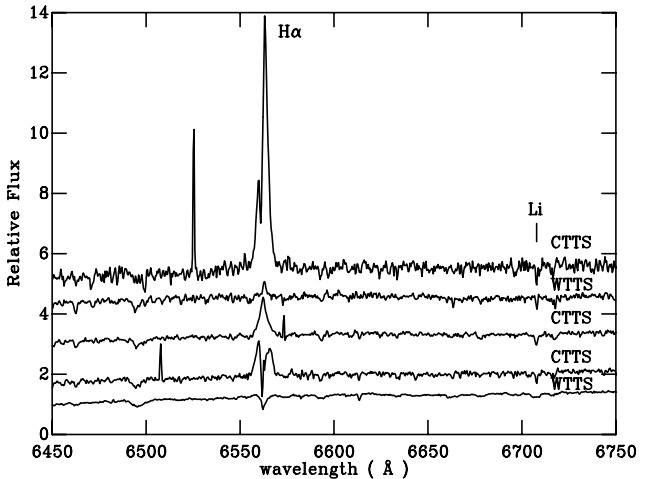


Figure 10. The spectra of the 5 TTS from the first configuration. From bottom to top, respectively: object 7 (field 2b), object 8 (field 2b), object 18 (field 1a), object 32 (field 2a), and object 49 (field 3b).

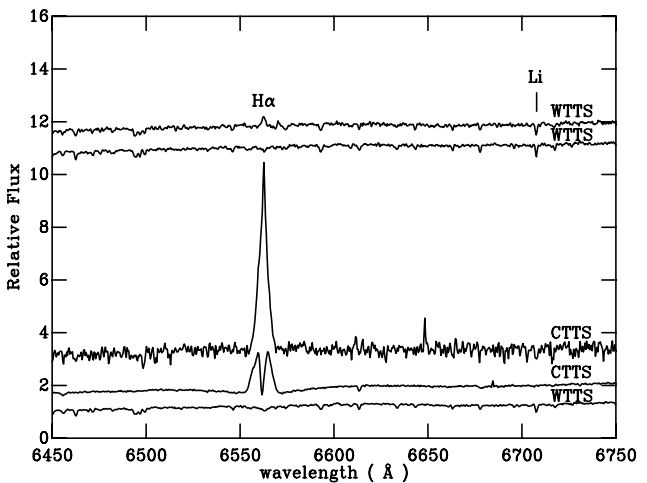


Figure 11. The spectra of the 5 TTS from the second configuration. From bottom to top, respectively: object 81 (field 3b), object 84 (field 3b), object 95 (field 1a), object 100 (field 2b), and object 106 (field 1a). Note that object no. 84 is the veiled CTTS for which we do not have a RV measurement: the extension of the wings on both sides of the H α line suggests a strong T Tauri wind.

were masked before performing the cross-correlation. In the case of double peaks in the cross-correlation function, the cross-correlation was repeated in the region 6650-6800 Å: if both peaks were still separated (indicating a possible binary nature of the object), we fit a double Gaussian to find the shifts (and hence RVs) for both of them. In total we were able to obtain RV measurements for 74 objects. Of the 36 targets without RV determinations, 15 are earlier type A and F stars, while the rest have relatively noisy spectra.

From repeat measurements of a number of targets taken for a different programme on the same observing run, we estimate a RV accuracy of $\pm 3 \text{ km s}^{-1}$. The relative RVs were placed in the heliocentric reference frame.

Radial velocity measurements allow us to find candidate kinematic members of the Cep OB3 association. We consider to be likely members all those stars with RV values within 2 sigma ($= 6.0 \text{ km s}^{-1}$) of the Cep OB3 mean RV value $-22.5 \pm 1.5 \text{ km s}^{-1}$ (derived from already known members; Garmany 1973), i.e., in the range -28.5 to -16.5 km s^{-1} . Out of 74 objects with measured RV, we found 21 stars in total as candidate kinematic members and 53 kinematic non-members. We can estimate the likely number of contaminants to have the correct RV by chance. Assuming for the 53 kinematic non-members a uniform spread over about 190 km s^{-1} velocity space, then we would only expect about $53 * 12/190 = 3.3 \pm 1.8$ objects to fall by chance in our selection range of $\pm 6 \text{ km/s}$. Therefore, out of 21 candidate kinematic members, we would expect about 3 ± 2 objects to have the correct RV by chance and 18 ± 2 objects to be true association members.

5.4 Li I and H α equivalent widths

The Li I ($\lambda 6707.8$) and H α ($\lambda 6563$) EWs were measured using the Starlink DIPSO package. The EW was measured by integration below a linear continuum between the two extremes points of the specified line. Each EW was measured three times (because of possible uncertainties in the continuum placement), and a mean value determined. The mean estimated errors are of about $20 \text{ m}\text{\AA}$ and 0.2\AA respectively for Li I and H α EWs, as a result of uncertainty in the continuum location.

Note that at our resolution the Li I 6708 \AA line cannot be separated from an Fe I line at 6707.4 \AA , although strong Fe I lines at 6705 \AA , and 6710 \AA are clearly resolved. However, the likely strength of the 6707.4 line for F- to K-type stars would be $\leq 25 \text{ m}\text{\AA}$ – its EW being estimated from the empirical relationship $[20(B-V)_0 - 3] \text{ m}\text{\AA}$ given by Soderblom et al. (1993).

By comparing the spectra with the library of stellar spectra given by Jacoby, Hunter & Christian (1984), we can also give a rough spectral classification for the objects. In Figs. 10 and 11, a montage of some of the extracted spectra is presented. The objects shown are all PMS stars according to our classification method (see below).

In Fig. 12, we plot the 49 stars for which we have both measured Li I 6707.8 \AA EWs and RVs, marking out the range for kinematic membership specified in Section 5.3. For the other 25 stars with measured RV we cannot detect an Li I feature (5 of these have RVs qualifying them for membership of Cep OB3b). Data on the 21 objects that have a RV consistent with membership of Cep OB3b are listed in Table 4. We give their coordinates, RVs, photometric values, Li and H α EWs, spectral types, class and correlation with a *ROSAT* X-ray source of NF99.

For those stars with measurable Li I absorption, we can set a minimum EW above which classification as a definite PMS object can be considered. A limit of $200 \text{ m}\text{\AA}$ is chosen for K stars, following the scheme proposed by Martín (1997). This is the EW expected for a K0 star just leaving the PMS phase of evolution. For M stars the EW associated with this transition is about $500 \text{ m}\text{\AA}$. We find 9 kinematic members with a Li I EW $> 200 \text{ m}\text{\AA}$: since these are all K-type stars, we can accept them as Cep OB3b PMS members. Data on the 12 remaining kinematic members of the association are

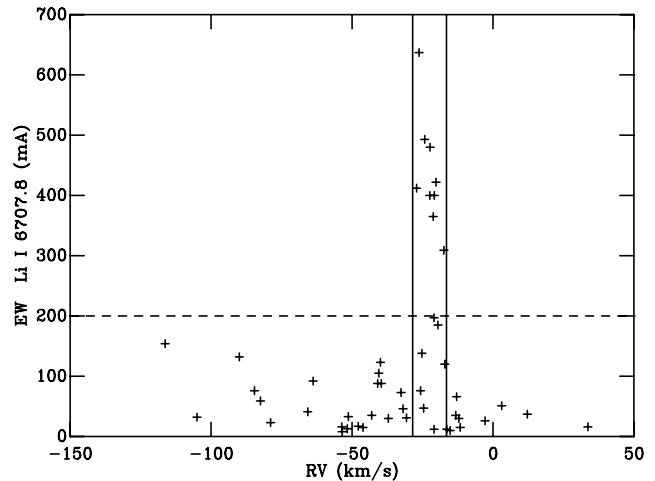


Figure 12. The 49 objects for which we have a RV measurement and which show Li I 6708 in absorption. The vertical lines define the RV range appropriate to members of the Cep OB3b subgroup. Objects above the dashed horizontal line at $200 \text{ m}\text{\AA}$ are definite K-type PMS stars. Those below are all F and G type stars, apart from one K-type star with a Li I EW of $197 \text{ m}\text{\AA}$. Note that objects with only upper limits for Li I 6708 absorption are not shown.

given in the lower part of Table 4. Two of these stars (no. 13 and 69) are K stars with insufficient Li EW to be considered as young PMS objects (note however that no. 13 only misses the $200 \text{ m}\text{\AA}$ limit by $3 \text{ m}\text{\AA}$ so we consider it possible PMS as well). The remaining 10 are F- or G-type stars. There are 6 of them which are “possible” PMS members, due to their spectral type and Li I absorption. For spectral types earlier than K the empirically determined timescale for Li depletion becomes long enough that an EW indicating essentially undepleted Li is no longer a guarantee of PMS status, but merely means the star is young (say less than a few hundred Myr). However if the Li EW is significantly less than expected for undepleted photospheric Li, then a PMS status can be ruled out. The appropriate EW thresholds can be judged from measurements in young open clusters like the Pleiades (Soderblom et al. 1993) and are $100\text{--}200 \text{ m}\text{\AA}$ for G-type stars, $50\text{--}100 \text{ m}\text{\AA}$ for F-type stars and perhaps even no detection of the Li line at all for stars of type F0 or earlier. Note that we do not consider object no. 50 in Table 4 as a possible PMS star: it is F-type with a Li EW which could just be consistent with undepleted Li; its $(V - I)_0$ is about 0.35 mag and thus $E(V - I) = 2.5$, hence implying an A_V value of ~ 6 which is much higher than any other extinction value reported for known Cep OB3b members.

In total we find 16 objects which are likely to be Cep OB3b PMS members - reasonably consistent with our expectations from the RV measurements (see Section 5.3) which predicted about 18 ± 2 objects to be true association members.

The EW of the H α line can be used to further classify a PMS object as a CTTS or WTTS. In fact, although its Li I EW can be small because of optical veiling (responsible for a masking of the absorption lines; see for example Basri, Martín & Bertout 1991), a CTTS can be immediately recognised by its very wide and strong H α emission which cannot be explained by means of stellar chromospheric activity only

Table 4. The candidate PMS and possible PMS members of Cep OB3b found with the present investigation.

#	field	RA (J2000.0)	Dec (J2000.0)	RV _{hel} (km s ⁻¹)	V	(V-I)	EW(Li I) (mÅ)	EW(H α) (Å)	sp. type	class	X-ray (NF99)
7 ^a	2b	22 56 38.721	+62 37 14.43	-24.2	14.548	2.264	493	1.1	K	WTTS	X34
8	2b	22 56 28.955	+62 38 41.49	-20.2	16.733	2.347	422	-5.9	K	CTTS	
18	1a	22 56 20.132	+62 52 23.16	-22.3	16.789	2.444	480	-6.2	K	CTTS	X26
32	2a	22 54 07.285	+62 53 42.23	-27.1	16.939	2.113	412	-0.9	K	WTTS	
49 ^b	3b	22 53 03.636	+62 37 08.27	-20.8	(b)	(b)	400	-27.3	K	CTTS	
81	3b	22 52 11.102	+62 29 46.71	-17.4	15.676	2.113	309	0.5	K	WTTS	
84 ^c	3b	22 52 50.152	+62 27 33.83	:	15.626	2.013	:	-13.4	K	CTTS	
95	1a	22 55 59.654	+62 47 45.08	-26.2	17.128	2.626	637	-28.4	K	CTTS	X20
100	2b	22 55 25.087	+62 36 51.35	-21.2	16.180	2.028	365	0.3	K	WTTS	
106	1a	22 56 29.678	+62 45 28.68	-22.4	15.660	1.960	400	-0.8	K	WTTS	X29
13	1a	22 55 17.649	+62 43 23.43	-20.9	15.783	1.593	197	0.8	K	PMS?	
16	1a	22 56 05.055	+62 48 27.26	-25.2	15.912	1.543	138	2.4	G	PMS?	
36	3b	22 51 52.222	+62 38 51.49	-19.5	15.670	2.108	185	1.4	G	PMS?	
101	2b	22 56 29.791	+62 38 53.76	-17.1	15.727	2.395	120	2.1	F	PMS?	
10	2a	22 54 51.609	+62 41 52.40	-25.7	15.004	1.962	76	4.2	F	PMS?	
56	3a	22 51 04.777	+62 49 25.35	-20.9	16.853	2.180	12	2.3	G		
69	4a	22 50 58.865	+62 36 50.63	-24.6	15.553	1.511	47	1.0	K		
12	1a	22 56 39.087	+62 45 09.36	-20.3	14.910	1.892	< 10	3.6	F	PMS?	X35
38	3b	22 52 20.510	+62 38 05.39	-27.0	14.770	1.259	< 10	1.3	G		
40	3b	22 50 52.516	+62 52 05.88	-23.7	16.920	2.116	< 10	1.2	G		
50	3b	22 51 45.635	+62 27 32.94	-27.3	14.676	2.841	< 10	3.6	F		
76 ^d		22 50 22.26	+62 25 21.6	-24.1			< 10	1.7	G		

^a This object is cross-correlated with BHJ40-096 (J96). According to NF99, it is K-type and has EW(Li I) = 380 mÅ and EW(H α) = 0.6 Å, whereas we find values about 30 and 80 per cent larger.

^b This is a PMS object (CTTS), but, unfortunately, it is on a bad column on the CCD image and so it has a non-zero flag (see Naylor et al. 2002), therefore we cannot trust its V (= 16.030) and (V-I) (= 1.867) photometric colours.

^c We also consider this object to be a kinematic member, even though we do not have its RV measurement, because of its CTTS nature; and it is clearly veiled.

^d This is a star falling down a sky fibre, for which we do not have optical photometry.

Table 5. Profiles and velocity width of the H α emission line for the PMS members.

#	class	type ^a	V _{Hα} (km s ⁻¹) (FWZH) ^b
7	WTTS		460
8	CTTS	II-R	630
18	CTTS	I	630
32	WTTS	III-B	260
49	CTTS	III-B	620
81	WTTS		430
84	CTTS	II-B	830
95	CTTS	I	670
100	WTTS		410
106	WTTS	I	260

^a From Reipurth et al. (1996) scheme: I for symmetric profiles with no or weak absorption features; II for double peak profiles, with the secondary peak more than half the strength of the primary one; III for double peak profiles with the secondary peak less than half the strength of the primary peak. B and R define the location of the secondary peak with respect to the primary (i.e., blue-wards or red-wards).

^b FWZH = full-width at zero height

(e.g., T Tauri winds, active accretion discs, or magnetic accretion columns; see Appenzeller & Mundt 1989; Hartmann, Hewett & Calvet 1994). Therefore it must show an emission H α EW larger than that expected from chromospheric emission for its spectral type. Conservative EW emission values proposed by Martín (1997; see also references therein) are: greater than 5 Å for K-type stars, 10 Å for early M-type stars, and 20 Å for late M-type stars. On this basis, we can classify 4 of the 9 definite PMS candidates (with Li I EW > 200 mÅ) as CTTS, the other 5 PMS stars are WTTS. None of the remaining 6 “possible” PMS stars show strong H α emission.

Note that another K star (no. 84 in Table 4), without a useful RV and Li I EW measurement because it is so heavily veiled, can be classified as CTTS in Cep OB3b as well, by virtue of its extremely strong H α emission.

The spectra of these 5 CTTS and 5 WTTS are shown in Figs. 10 and 11.

We checked the velocity width of the H α emission lines in the 10 TTS and found that they were much larger than any plausible amount of rotational broadening (see Table 5; the typical error is about 9 km s⁻¹). From the strength of the line in each of them (full-width at zero height) we can say that possible problems in the sky subtraction procedure are not going to change the results of our classification (any sky

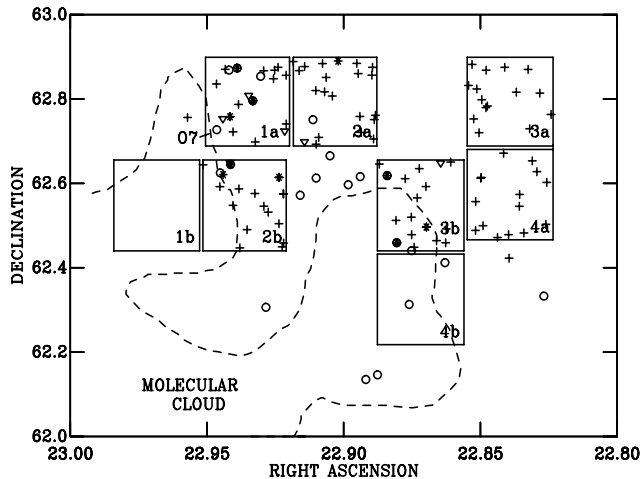


Figure 13. The spatial distribution of the 16 PMS objects in the Cep OB3b subgroup (symbols as in Fig. 4). The 5 CTTS and 5 WTTs are shown as filled circles and asterisks respectively. The 6 possible PMS stars are shown as open triangles. Note that one of the possible PMS stars is hidden behind the CTTS in field 2b. The remaining 94 spectroscopic objects are shown as black crosses (note that two of them fall outside our CCD fields: they are stars which fell down a sky fibre).

line contamination is unresolved at $\text{FWHM} \sim 50 \text{ km s}^{-1}$). In general, the spectroscopic targets having $\text{H}\alpha$ in emission show single-peaked as well as more complex profiles. A classification in these terms is also given in Table 5, using the scheme established by Reipurth, Pedrosa & Lago (1996).

We note that out of 10 definite TTS, just 4 (2 WTTs and 2 CTTS) have a *ROSAT* X-ray counterpart in NF99. Although the NF99 survey was not very sensitive, the low fraction of detections is an example of how an X-ray selected sample can be incomplete compared to optically-selected samples, unless the original X-ray survey is deep enough to sample the entire X-ray luminosity function of PMS stars in the considered mass range.

Out of 74 targets with measured RVs, there are 9 TTS plus a further 6 possible PMS stars which are Cep OB3b kinematic members and 53 non-members: this suggests that the contamination in the optically-selected PMS sample is of order 70 per cent. However, this large percentage is most likely the consequence of the generous region over which the targets were initially selected in the V versus V-I CMD.

The location of the CTTS, WTTs and possible PMS stars with respect to known Cep OB3b members is given in Fig. 13. Also plotted there are the remaining 94 spectroscopic objects. This confirms that low-mass PMS stars may indeed form close to higher-mass companions. The confirmed TTS seem to be spread in all the fields other than 3a and 4a, which are the most distant from the CO contour of the molecular cloud. Note, however, that these are small-number statistics and that we are biased against the detection of TTS in fields 3a and 4a simply by the field of view and spatial distribution of allocated fibres in the WYF-FOS configurations.

By means of the spectroscopic identification of at least 9 T-Tauri stars with the appropriate RVs, we have confirmed

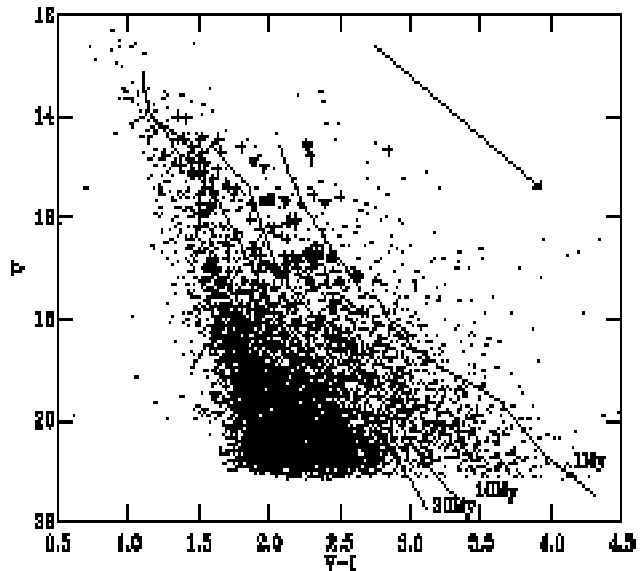


Figure 14. The colour-magnitude diagram in V versus (V-I) for the stars in the six fields used for the selection of the PMS sample for the spectroscopic follow-up. CTTS and WTTs from the spectroscopic follow-up are shown as filled circles and asterisks respectively. The remaining Cep OB3b kinematic members which are possible PMS stars are shown as open triangles. The other objects which were spectroscopically observed are shown as black crosses (two stars which fell down a sky fibre and for which we do not have photometric data are not shown). Note that a possible PMS object is hidden behind the WTTs at $V = 15.7$ mag and $(V-I) = 2.1$ mag; and one CTTS is not shown because we do not trust its photometric colours. Also plotted there are isochrones for 1, 10 and 30 Myr (Siess et al. 2000) and the average reddening vector for Cep OB3b (see Section 3).

the presence of low-mass stars associated with the younger subgroup of the Cep OB3 association.

6 THE AGE OF THE TTS OBJECTS

How old are the PMS objects in Cep OB3b? Is there an age gradient across the Cep OB3b subgroup? To answer these questions we have to compare the V versus (V-I) CMDs for different fields by means of isochrone fitting. If one can fit the PMS stars in one field with different isochrones, the most tempting conclusion would be a spread in ages. However, as we discuss below, there are several other factors which could contribute to such a spread.

Isochrones were computed from the evolutionary models of Siess, Dufour & Forestini (2000), using a metallicity of $Z=0.02$ and masses in the range $0.2 < M/M_{\odot} < 3.0$. To convert the effective temperatures resulting from their models to colours, we chose to use the conversion table of Siess, Forestini & Dougados (1997). In Figs. 14 and 15 we plot isochrones corresponding to 1, 10 and 30 Myr, applying the mean extinction ($A_V = 2.81$), colour excess ($E(V-I) = 1.18$) and distance modulus ($dm = 9.65$) for Cep OB3b (see Section 3).

Figure 14 shows the location of both the TTS and the possible PMS Cep OB3b kinematic members in the V versus (V-I) colour-magnitude diagram. Also shown there are the

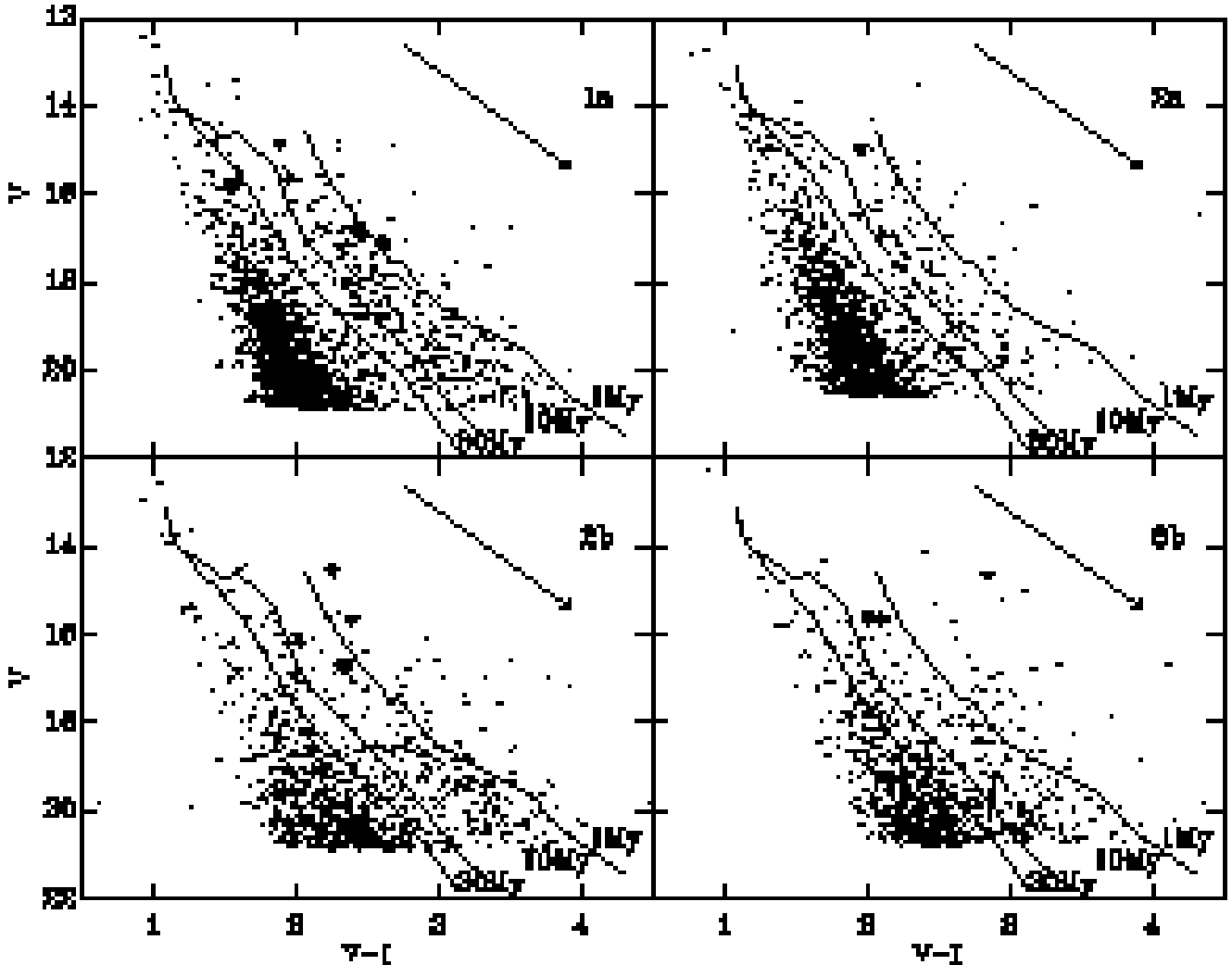


Figure 15. Isochrones for 1, 10 and 30 Myr (Siess et al. 2000) for fields 1a (top-left), 2a (top-right), 2b (bottom-left) and 3b (bottom-right). CTTS and WTTS are shown respectively as filled circles and asterisks. The remaining Cep OB3b kinematic members which are possible PMS stars are enclosed by open triangles. Note that 1 CTTS belonging to field 3b is not plotted because we do not trust its photometric colours (see footnote b in Table 5). Furthermore, note that a possible PMS object in field 3b is hidden behind the WTTS. And finally, always in field 3b, the open triangle which is not centred on a data-point is a possible PMS object which is flagged in our catalogue (and therefore not appearing in the plot), but which was included in the sample for the spectroscopic-follow up due to its possible binary nature: it is a close visual binary on the CCD image (and indeed a close examination of the cross-section of the CCD image revealed that it is double peaked), but it is not a spectroscopic binary. Also plotted there is the average reddening vector for Cep OB3b (see Section 3).

remaining objects which were spectroscopically followed-up (apart from two stars which fell down a sky fibre and for which we do not have photometric data). It can be seen in this diagram that the 6 possible PMS stars are more widely scattered in $(V-I)$ than the TTS, with a few sitting in the locus of the background sequence. At the same time, the V magnitudes for this group occupy a similar range to the TTS despite the group's much earlier mean spectral type. Given the uncertainty over the status of this group, we restrict further discussion to the definite TTS only.

In field 1a (see Fig. 15 [top-left]) the TTS objects are likely to be 1-10 Myr old, in agreement with the age (~ 7 Myr) determined for the OB-type members. More precisely, the 2 CTTS (shown as filled circles) lie close to the 1 Myr isochrone, whereas the WTTS (shown as an asterisk) lies

closer to 10 Myr. Note that there is a lack of stars between the 10-30 Myr isochrones: this clearly defines the PMS locus in the CMD – the bulk of stars occupying the region between the 1-10 Myr isochrones with a few at even younger ages. We have repeated the analysis using empirically calibrated isochrones from the D'Antona & Mazzitelli (1997) models, which yield slightly younger ages.

In Field 2a (see Fig. 15 [top-right]) we have just 1 WTTS, just less than 10 Myr old, suggesting an age similar to that of the WTTS in field 1a. Again, the interval between the 1-10 Myr isochrones is more populated than the interval between the 10-30 Myr isochrones.

In field 2b (see Fig. 15 [bottom-left]) we have 1 CTTS showing an age of about 1-5 Myr and 1 WTTS closer to 10 Myr old, in agreement with those found in field 1a; but there

is also a WTTS that appears to be less than 1 Myr old. This WTTS could be as young as this, but a 0.8 mag difference in its visual magnitude could also perhaps be explained as due to binarity, photometric errors and spread in distance (discussed below). Variations in extinction or the value of R are unlikely to be of assistance. The reddening vector is close to parallel to the isochrones, whilst an anomalously large value of R would steepen the reddening vector and lead to an even younger age (see Section 3). If we look at its position with respect to the Cep OB3b subgroup (see Fig. 13 and Table 5), we can see that this object is closer to the molecular contour and to the early-type member BHJ 40: although a larger A_V value would be plausible because of its proximity to the molecular material, this seems not to be the case given that BHJ 40 has an extinction of just ~ 3 mag. In field 2b there seems to be no clear difference in the stellar densities of the gaps between the 1-10 Myr and the 10-30 Myr isochrones: we think that the 10-30 Myr gap is filled by some objects of the background population suffering higher extinction, since the bulk of the background sequence in this field appear to lie at redder (V-I) colours than that in field 1a. In Appendix B we report the additional extinction necessary to match the background sequence in field 2b with that of field 1a.

Finally, in field 3b (see Fig. 15 [bottom-right]), there are 1 CTTS and 1 WTTS at about the same age of $\simeq 5$ Myr. Note that 1 CTTS belonging to this field is not plotted because we do not trust its photometric colours (see footnote b in Table 5). These two TTS are even closer to the cloud than the TTS of field 2b (see Fig. 13 and Table 5). However, an anomalous R value for these two objects, which would give an even younger age, is once again unlikely: the extinction for BHJ 10 (an early-type member falling in this field) is $A_V \simeq 2.5$, a little less than the adopted extinction. As in field 2b, there is no clear gap between the 10-30 Myr isochrones: this effect is again probably caused by contamination from the background sequence, pushed to even redder colours than in field 2b (see Appendix B). Furthermore, there seem to be somewhat more objects in this field which lie on the red side of the 1 Myr isochrone.

It is not easy to assess the vertical spread around the isochrones in each of the fields 1a, 2a, 2b and 3b respectively. In fields 2b and 3b the contamination from background objects complicates the picture, and it also seems that there are many objects at even younger ages (< 1 Myr). These objects could be early-type PMS stars very deeply embedded in the molecular cloud than the TTS objects we have discovered, i.e., suffering an higher extinction than the mean adopted value of 2.81, but the extinction vector runs nearly parallel to the isochrones, so this seems unlikely (see below). A higher value of R would make these objects even younger. Neither are these stars likely to be foreground contaminants. The CMDs of fields 1b and 4b which are pointing at the molecular cloud do not show many stars in this portion of the colour-magnitude diagram. We suspect therefore that there are genuine, very young low-mass PMS stars in Cep OB3b. However, from Fig. 14 we can see that this possible < 1 Myr population has not yet been adequately probed with spectroscopy, whereas we *can* rule out a significant population of > 10 Myr objects, because we have sampled this area of the CMD quite well.

If we consider fields 1a and 2a, the separation between

background and PMS loci are clearly defined. The photometric data alone suggest a spread of ages between < 1 and 10 Myr, but this is not contradicted by the position in the CMDs of the small number of spectroscopically confirmed TTS (see Fig. 15, top). This corresponds to a vertical spread of 1.5 magnitudes in V. This is more than the spread expected from the presence of unresolved binaries (0.75 mag) plus our photometric errors for V (less than a hundredth of a mag up to $V=17.5$, and ~ 0.05 up to $V=20.0$). If we also allow for a spread in distance, which is at most 0.1 mag for the Cep OB3b members within our fields, we could perhaps explain a 0.9 mag spread.

It would then be tempting to explain the remaining 0.6 mag difference as the effect of extinction variations. However, we stress again that the reddening vector runs almost parallel to the 1 Myr isochrone and therefore it is difficult to explain such a difference with a change in the extinction value. A scatter of R between values of 3 and 5 would introduce a horizontal scatter of about 0.2 in $V - I$ and hence about 0.5 in V , but there really is no concrete evidence that such a scatter is present from the spectroscopic work on the early-type association members. Note that Preibisch & Zinnecker (1999) found a similar PMS CMD for stars in the Upper Sco OB association, with a spread of about 1.2 mag, which they explained as the effect of unresolved binaries, photometric errors and spread in distance. They concluded by saying that a small spread in ages cannot be excluded, but that it is probably not larger than about 2 Myr. Dolan & Mathieu (2001) found instead a real age spread in the λ Orionis PMS population. Similarly, our results strongly suggest the possibility of a real spread in ages for the low-mass stars in the Cep OB3b subgroup. However, a larger spectroscopic sample is really needed to confirm this hypothesis.

7 DISCUSSION

We have photometrically surveyed the younger subgroup of the Cep OB3 association, Cep OB3b, at optical wavelengths (see Sections 2 and 3) and followed-up spectroscopically an optically-selected PMS sample (see Section 5). As a result, we have discovered 10 TTS kinematic members of the association and a further 6 objects that are very likely association members. Isochrone fitting (see Section 6) to these objects suggests ages from < 1 to nearly 10 Myr, probably compatible with the OB-type members of the subgroup. Furthermore, we have found that binarity, photometric errors, spreads in distance and in extinction (as suggested by the early-type members of the younger subgroup) are unlikely to fully explain the spread of objects around the 1 Myr isochrone in the CMDs. Unless there are large variations in R or visual extinction, for which there is no evidence from the early-type stars in the region, then we have a quite strong suggestion of a significant age spread in Cep OB3b. Unfortunately, our spectroscopic sample is small and in particular does not adequately sample the photometric association candidates with apparent ages of < 1 Myr.

In the Introduction we anticipated speculations about how star formation is proceeding in the Cep OB3 association, i.e., following the sequential model of Elmegreen & Lada (1977) or as the result of a supernova explosion. The sequential model would predict: bursts of star formation oc-

curing every few Myr, about 10-50 pc apart; a substantial amount of gas near the younger subgroup, but none (or very little) in the older subgroup; a velocity difference between the two subgroups (or gas velocity, or both) in the range 5–10 km s⁻¹. This is effectively what is occurring in the Cep OB3 association, with: a temporal separation between the older and the younger subgroup of about 3 Myr and a spatial separation of about 13 pc (Sargent 1979); the younger subgroup is closer to the molecular cloud (Blaauw 1964); and there is a velocity difference of about 4 km s⁻¹ (Garman 1973) between the two subgroups. Unfortunately our spectroscopic sample is too sparse to be useful for a detailed comparison. All we can say is that the confirmed PMS objects in fields 1a, 2a, 2b, and 3b are between 1 and 10 Myr old. In addition, field 3b shows more young objects less than 1 Myr old, potentially implying that star formation in field 3b ended later than in field 1a.

Thus the photometric evidence leads us to marginally favour a “contemporaneous” model of star formation in the younger subgroup of the Cep OB3 association, i.e., of star formation possibly triggered by a supernova explosion. As suggested in the Introduction, the pulsar PSR 2324+60 of Assousa et al. (1977), some 10 Myr old, seems to be the possible stellar remnant of a SN event, as testified by the presence of a H I expanding shell centred in the older subgroup. Its location close to the easternmost fields could also explain why star formation in the westernmost fields ended later, although another possibility for terminating star formation is discussed below. Certainly the easternmost fields are closer to the major source of ionising radiation in the younger subgroup, i.e., the O7n star: a more plausible explanation for the likely age spread would then be that this star may have made star formation more difficult in the recent past by dispersing the shielding molecular material from its neighbourhood.

In total, we have found 10 TTS in the Cep OB3b subgroup, divided into 5 CTTS and 5 WTTS. From the numbers of WTTS and CTTS, we can derive the WTTS/CTTS ratio, a very important number in addressing the problem of the dissipation timescales for circumstellar discs. The value for the WTTS/CTTS ratio presented in the literature changes significantly in different star-forming regions. In T associations it is in the range 1-13. In particular, WTTS/CTTS values from 1 (central region) to > 8 (wider region), 2-8, 4 and 13 were found respectively in Taurus-Auriga (Neuhäuser et al. 1995; Hartmann et al. 1991), Chamaeleon (Feigelson et al. 1993; Alcalá et al. 1995), ρ Ophiuci (Martín et al. 1998) and Lupus (Krautter et al. 1997). All these studies are based on an optical spectroscopic follow-up of X-ray selected samples, except for the study of Hartmann et al. (1991) which is based on a proper motion selected sample. Note however that these *Einstein* or *ROSAT* X-ray selected samples are biased towards WTTS, because CTTS are more difficult to detect in soft X-rays, and therefore the true WTTS/CTTS ratio may be even smaller.

There are not so many determinations of the ratio between TTS subtypes in OB associations. To our knowledge, the only two for which the fraction of WTTS on CTTS has been determined (on the basis of the strength of their H α emission lines) are the Orion and Upper-Scorpius OB associations. In these regions, the low-mass PMS populations have about the same age ($\sim 6-7$ Myr and ~ 5 Myr respectively).

From an optically-selected sample followed by optical spectroscopy, Dolan & Mathieu (1999) found a WTTS/CTTS ratio of 17 in λ -Ori. Recently, Dolan & Mathieu (2001) found a WTTS/CTTS ratio of 35 in the central region of λ -Ori, from an optical photometric survey followed up by multi-object spectroscopy. In Upp-Sco, Walter et al. (1994) found a WTTS/CTTS ratio of 14 from an Einstein Observatory X-ray selected sample of PMS stars, together with optical spectroscopic and optical and NIR photometric follow-up. Preibisch & Zinnecker (1999) found a WTTS/CTTS value of 24 (just 4 CTTS retaining their discs against 94 WTTS) from an X-ray selected sample (*ROSAT* All Sky Survey and Einstein Observatory) of stars in the same region, followed by optical spectroscopy and photometry; a 2dF optical spectroscopic follow-up has recently revealed 98 new low-mass PMS stars in a 6 square degree field in the association, with a WTTS/CTTS of 9 (Preibisch et al. 2001).

The WTTS/CTTS ratio of 1 we have found for Cep OB3b is closer to the value known for T associations than OB associations. Furthermore, although our sample is small we can rule out a value of 9 or more (which all the above OB associations have) at the 99.8 percent confidence level. We stress that our ratio is worked out from the spectroscopic follow-up of an optically-selected PMS sample, therefore it is not biased against WTTS. Furthermore we deliberately chose our spectroscopic sample from a large area of the CMD to avoid any age bias.

The explanation of such a low WTTS/CTTS value for Cep OB3b could be ascribed to a less effective erosion (through stellar winds and ionising radiation) of the circumstellar discs around the low-mass PMS members by the high-mass members of the association. The kinematic age of < 1 Myr found by a number of authors (see Section 1) probably indicates when much molecular material was lost and the association became unbound, i.e., the bulk of the molecular material shielding the newly-born low-mass stars from the dispersive influences of the high-mass stars has only been recently cleared. An interesting speculation is that this transition was triggered by the supernova event centred on Cep OB3a that occurred less than a million years ago (Simonson & van Someren Greve 1976) and that it terminated low-mass star formation.

The age of the low-mass PMS stars we have found in Cep OB3b is suggesting disc lifetimes of about 5 Myr. Low-mass stars remain in the protostellar phase until an external trigger obliges them to cross the birthline through the collapse of the protostellar core and the dispersion of the protostellar envelope. At that time they become optically visible and then, and only then, their isochronal clock is set to 0. At an age of about 1 Myr they are visible as T Tauri stars: approximately half of them are still surrounded by accretion discs (Strom, Strom & Merrill 1993; Edwards 1993, and references therein) which can survive as long as 10 Myr (see Strom et al. 1989; Skrutskie et al. 1990; Preibisch & Zinnecker 1999). Recently, Haisch, Lada & Lada (2001a) reported the results of the L-band survey of the clusters NGC 2264, NGC 2362 and NGC 1960 (of intermediate age, 2.5-30 Myr), using JHKL colours to obtain a census of the cluster objects with a circumstellar disc. Coupled with previous studies on other clusters, i.e. NGC 2024 (Haisch et al. 2001), Trapezium (Lada et al. 2000) and IC 348 (Haisch, Lada & Lada 2001b), the results suggest that the disc fraction in a

cluster is initially very high (> 80 per cent), and rapidly decreases as the cluster age increases; that about half the stars in the cluster lose their discs in less than about 3 Myr; and finally that all the cluster members lose their discs in about 6 Myr or more. All these papers use NIR excess as marker of circumstellar discs, but not all stars showing such an excess are strong H α emitters. The fact that we have detected the presence of accreting discs in 50 per cent of TTS systems is a lower limit to the NIR excess disc fraction in Cep OB3b. The CTTS we have found are all less than 5 Myr old, consistent with the disc lifetime limits found by Haisch, Lada & Lada (2001a).

8 CONCLUSIONS

Thanks to an optical CCD photometric survey, we have discovered low-mass PMS stars in the younger subgroup of the Cep OB3 association, Cep OB3b. Their presence has been confirmed by spectroscopic follow-up of an optically-selected PMS sample. Out of 110 stars for which we have spectra, we classified 10 PMS and 6 possible PMS objects, all of which are kinematic members of the association. Just 4 of the PMS objects have *ROSAT* X-ray counterparts, suggesting the presence of a substantial, less X-ray-active population. Thus the *ROSAT* X-ray selected sample is likely to be highly incomplete. Forthcoming, more sensitive *Chandra* observations will probably uncover a much larger X-ray emitting population.

Among the PMS members, we found 5 CTTS and 5 WTTS with likely ages ranging from about < 1 and nearly 10 Myr and masses in the range $\sim 0.9 - 3.0 M_{\odot}$. It is difficult to explain the apparent age spread of PMS objects around the isochrones solely by means of unresolved binaries, photometric errors, spreads in distance and extinction. If the objects which appear younger than 1 Myr are real Cep OB3b members, the spread would be broad enough to confirm a real spread in ages across the subgroup: a spectroscopic follow-up for the very young candidate association members is therefore needed to investigate this and confirm that low-mass star formation has only recently ended in Cep OB3b.

The fact that there seem to be objects with photometric ages younger than 1 Myr in the westernmost fields of the subgroup could be explained as the result of star formation triggered by a supernova explosion. Indeed there is evidence for a SN remnant in the older subgroup of the association that happened closer to the easternmost fields. This would explain why star formation in the westernmost fields appears to be ended later. Another possible explanation would be the proximity of the easternmost fields to the major ionising source in the region – the O7n star.

From the number of the newly discovered CTTS and WTTS the WTTS/CTTS ratio is equal to 1. Despite the presence of OB type members, this value is closer to that found in T associations (1-13) than to that found in OB associations (up to 20). This suggests that the stellar winds and ionising radiation from the high-mass members of the association were less effective in eroding and subsequently evaporating the circumstellar discs around the low-mass members of Cep OB3b. We speculate that it is probably due to the

quite recent dispersal of shielding molecular material in the association.

Further spectroscopy is urgently required to test these scenarios. In addition, the forthcoming availability of 2MASS near infrared data over the whole of our surveyed field will enable us to better isolate the PMS populations and put further constraints on the presence and timescales for dissipation of circumstellar material (Pozzo et al. in preparation).

ACKNOWLEDGEMENTS

This research has made use of the US Naval Observatory A2.0 catalogue. The Isaac Newton Telescope is operated on the island of La Palma by the Isaac Newton Group in the Spanish Observatorio del Roque de los Muchachos of the Instituto de Astrofísica de Canarias. MP was supported by a Departmental Research Studentship in Keele University during her PhD and is currently supported by a PPARC Postdoctoral Research Fellowship at Imperial College. TN was in receipt of a PPARC advanced fellowship when the majority of this work was carried out. We thank the referee, Leisa Townsley for a very thorough report.

REFERENCES

- Alcalá J.M., Krautter J., Schmitt J.H.M.M., Covino E., Wichmann R., Mundt R., 1995, A&AS, 114, 109
 Appenzeller I., Mundt R., 1989, A&AR, 1, 291
 Assousa G.E., Herbst W., Turner K.C., 1977, ApJ, 218, L13
 Basri G., Martín E.L., Bertout C., 1991, A&A, 252, 625
 Bastian U., Finkenzeller U., Jaschek C., Jaschek M., 1983, A&A, 126, 438
 Bertout C., 1989, ARA&A, 27, 351
 Blaauw A., 1964, ARA&A, 2, 213
 Blaauw A., 1991, The Physics of Star Formation and Early Stellar Evolution. Kluwer Academic Publishers, Dordrecht, p. 125
 Blaauw A., Hiltner W.A., Johnson H.L., 1959, ApJ, 130, 69 (BHJ). *Erratum*: 1960, ApJ, 131, 527
 Bouvier J., Cabrit S., Fernández M., Martín E.L., Matthews J.M., 1993, A&A, 272, 176
 Bouvier J., Covino E., Kovo O., Martín E.L., Matthews J.M., Terranegra L., Beck S.C., 1995, A&A, 299, 89
 Brown A.G.A., Dekker G., de Zeeuw P.T., 1997, MNRAS, 285, 479
 D'Antona F., Mazzitelli I., 1997, Mem. Soc. Astron. Ital., Vol. 68, p. 807
 de la Fuente Marcos R., 1995, A&A, 301, 407
 De Veig C., 1966, Z. Astrophys., 64, 268
 de Zeeuw P.T., Brand J., 1985, in Birth and Evolution of Massive Stars and Stellar Groups, W. Boland and H. van Woerden ed., (Dordrecht: Reidel), p. 95
 Dolan C.J., Mathieu R.D., 1999, AJ, 118, 2409
 Dolan C.J., Mathieu R.D., 2001, AJ, 121, 2124
 Edwards S. et al., 1993, AJ, 106, 372
 Elmegreen B.G., Lada C.J., 1977, ApJ, 214, 725
 Feigelson E.D., DeCampli W.M., 1981, ApJ, 243, L89
 Feigelson E.D., Montmerle T., ARA&A, 1999, 363
 Feigelson E.D., Casanova S., Montmerle T., Guibert J., 1993, ApJ, 416, 623
 Feigelson, E.D., Broos, P., Gaffney, J.A., Garmire, G., Hillenbrand, L.A., Pravdo, S.H., Townsley, L., Tsuboi, Y., 2002, ApJ, 574, 258
 Felli M., Tofani G., Harten R.H., Panagia N., 1978, A&A, 69, 199

- Fitzgerald M.P., 1970, *A&A*, 4, 234
- Flaccomio, E., Micela, G., Sciortino, S., 2003a, *A&A*, 397, 611
- Flaccomio, E., Damiani, F., Micela, G., Sciortino, S., Harnden, F.R. Jr., Murray, S.S., Wolk, S.J., 2003b, *ApJ*, 582, 382
- Gahm G., 1981, *The Universe at Ultraviolet Wavelengths* (NASA Conf. Pub. 2171), p. 105
- Garmany C.D., 1973, *AJ*, 78, 185
- Haisch K.E., Lada E.A., Lada C.J., 2001a, *ApJ*, 553, L153
- Haisch K.E., Lada E.A., Lada C.J., 2001b, *AJ*, 121, 2065
- Haisch K.E., Lada E.A., Piña R.K., Telesco C.M., Lada C.J., 2001, *AJ*, 121, 1512
- Harper C.L., 1996, *ApJ*, 466, 1026
- Harten R.H., Thum C., Felli M., 1981, *A&A*, 94, 231
- Hartmann L., Hewett R., Calvet N., 1994, *ApJ*, 426, 669
- Hartmann L., Jones B.F., Stauffer J.R., Kenyon S.J., 1991, *AJ*, 101, 1050
- Herbig G.H., 1962, *Adv. Astr. Astrophys.*, 1, 47
- Heyer M.H., Carpenter J.M., Ladd E.F., 1996, *ApJ*, 463, 630
- Jacoby G.H., Hunter D.A., Christian C.A., 1984, *ApJS*, 56, 257
- Johnson H.L., Morgan W.W., 1953, *ApJ*, 117, 313
- Johnstone D., Hollenbach D., Bally J., 1998, *ApJ*, 499, 758
- Jordi C., Trullols E., Rosselló G., Lahulla F., 1992, *A&AS*, 94, 519
- Jordi C., Galadí-Enriquez D., Trullols E., Lahulla F., 1995, *A&AS*, 114, 489 (J95)
- Jordi C., Trullols E., Galadí-Enriquez D., 1996, *A&A*, 312, 499 (J96)
- Kimeswenger S., Weinberger R., 1989, *A&A*, 209, 51
- Krautter J., Wichmann R., Schmitt J.H.M.M., Alcalá J.M., Neuhäuser R., Terranegra L., 1997, *A&AS*, 123, 329
- Lada C.J., Muench A.A., Haisch K.E., Lada E.A., Alves J.F., Tollestrup E.V., Willner S.P., 2000, *AJ*, 120, 3162
- Landolt A.U., 1992, *AJ*, 104, 340
- Lasker B.M., Sturch C.R., McLean B.J., Russell J.L., Jenkner H., Shara M.M., 1990, *AJ*, 99, 2019
- Martín E.L., 1997, *A&A*, 321, 492
- Martín E.L., Montmerle T., Gregorio-Hetem J., Casanova S., 1998, *MNRAS*, 300, 733
- Mathis J. S., 1990, *ARA&A*, 28, 37
- McCaughrean M.J., O'Dell R.C., 1996, *AJ*, 111, 1977
- Monet D.G., 1998, *BAAS*, 193, 120.03
- Montmerle T., Koch-Miramond L., Falgarone E., Grindlay J.E., 1983, *ApJ*, 269, 182
- Moreno-Corral M.A., Chavarría K.C., De Lara E., Wagner S., 1993, *A&A*, 273, 619
- Naylor T., 1998, *MNRAS*, 296, 339
- Naylor T., Fabian A.C., 1999, *MNRAS*, 302, 714 (NF99)
- Naylor T., Totten E.J., Jeffries R.D., Pozzo M., Devey C.R., Thompson S.A., 2002, *MNRAS*, 335, 291
- Neuhäuser R., Sterzik M.F., Schmitt J.H.M.M., Wichmann R., Krautter J., 1995, *A&A*, 295, L5
- Panagia N., Thum C., 1981, *A&A*, 98, 295
- Pollacco D., Bridges T.J., Rees P.C.T., Lewis J.R., Boyle B.J., Lewis I., King D.L., Telting J., Corradi R., 2000, *AUT-OFIB2/WYFFOS User Manual*
- Pozzo, M., Jeffries, R.D., Naylor, T., Totten, E.J., Harmer, S., Kenyon, M., 2000, *MNRAS*, 313, L23
- Preibisch T., Zinnecker H., 1999, *AJ*, 117, 2381
- Preibisch T., Guenther E., Zinnecker H., 2001, *AJ*, 121, 1040
- Rebull L.M., Hillenbrand L.A., Strom S.E., Duncan D.K., Patten B.M., Pavlovsky C.M., Makidon R., Adams M.T., 2000, *AJ*, 119, 3026
- Reipurth B., Pedrosa, Lago M.T.V.T., 1996, *A&AS*, 120, 229
- Särg K., Wramdemark S., 1970, *A&AS*, 2, 251
- Sargent A.I., 1977, *ApJ*, 218, 736
- Sargent A.I., 1979, *ApJ*, 233, 163
- Siess L., Dufour E., Forestini M., 2000, *A&A*, 358, 593
- Siess L., Forestini M., Dougados C., 1997, *A&A*, 324, 556
- Simonson S.C. III, van Someren Greve H.W., 1976, *A&A*, 49, 343
- Skrutskie M.F., Dutkevitch D., Strom S., Edwards S., Strom K.M., 1990, *AJ*, 99, 1187
- Soderblom D.R., Jones B.F., Balachandran S., Stauffer J.R., Duncan D.K., Fedele S.B., Hudon J.D., 1993, *AJ*, 106, 1059
- Stelzer B., Neuhäuser R., 2001, *A&A*, 377, 538
- Stocke J.T., Liebert J., Gioia I.M., Maccararo T., Griffiths R.E., Danziger I.J., Kunth D., Lub J., 1983, *ApJ*, 273, 458
- Strom K.M., Strom S.E., Edwards S., Cabrit S., Skrutskie M.F., 1989, *AJ*, 97, 1451
- Strom K.M. et al., 1990, *ApJ*, 362, 168
- Strom K.M., Strom S.E., Merrill K.M., 1993, *ApJ*, 412, 233
- Testi L., Olmi L., Hunt L., Tofani G., Felli M., Goldsmith P., 1995, *A&A*, 303, 881
- Trullols E., Jordi C., Galadí-Enriquez D., 1997, in *Proceedings of the ESA Symposium 'Hipparcos-Venice '97'*, Vol. 402, p. 299
- Ungerechts H., Umbanhowar P., Thaddeus P., 2000, *ApJ* 537, 221
- Verschuur G.L., 1973, *A&A*, 24, 193
- Walker A.R., 1985, *MNRAS*, 213, 889
- Walter F.M., Boyd W.T., 1991, *ApJ*, 370, 318
- Walter F.M., Kuhl L.V., 1981, *ApJ*, 250, 254
- Walter F.M., Vrba F.J., Mathieu R.D., Brown A., Myers P.C., 1994, *AJ*, 107, 692
- Walter F.M., Alcalá J.M., Neuhäuser R., Sterzik M., Wolk S.J., 2000, in *Protostars and Planets IV*, University of Arizona Press, Mannings V., Boss A.P. and Russell S.S. eds., p. 273
- Wichmann R., Krautter J., Covino E., Alcalá J.M., Neuhäuser R., Schmitt J.H.M.M., 1997, *A&A*, 320, 185
- Wichmann R., Bouvier J., Allain S., Krautter J., 1998, *A&A*, 330, 521
- Winkler H., 1997, *MNRAS*, 287, 481
- Wolk S., 1996, PhD Thesis, State University of New York
- Wouterloot J.G.A., Brand J., Burton W.B., Kwee K.K., 1990, *A&A*, 230, 21

APPENDIX A: CROSS-CORRELATION WITH JORDI'S CATALOGUE

The majority of the works in the literature on the Cep OB3 association, are studies of the BHJ stars classified by BHJ. Besides these, there are some authors who studied the Cep OB3 region from a general point of view. Särg & Wramdemark (1970) presented photoelectric photometry of early-type stars in a Milky Way field in Cepheus, and Jordi et al. (1992) performed Strömgren photometry for 45 stars in the association. We have not tried a cross-correlation with their catalogues, since all their observed stars are brighter than ours (respectively $V < 11.54$ and $V < 10.72$, whereas we have stars with $V > 12$).

We cross-correlated our optical catalogue with the catalogue of Jordi et al. 1995 (hereafter J95). They observed 1056 stars from 18 randomly selected fields in Cep OB3, 7 in the old and 11 in the young subgroup. Their catalogue contains stars with $V = 8 - 21$ mag, with complete photometry in all the colours down to $V = 15.5$ for just 130 stars.

In Fig. A1, the V versus $(V-I)$ colour-magnitude diagram derived from J95 is shown on the same scale as the one used in the plots of Figs. 3. By comparing it with the CMD we have for just the field 1a (see Fig. 3, top-left), we can see that the pre-main sequence is less defined, almost imperceptible. This is a dilution effect, due to the fact that their total number of stars is less than half the number we have in just one field, and that the objects belong to fields

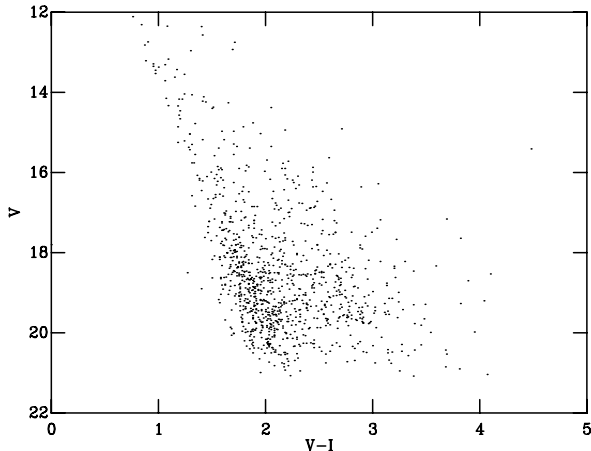


Figure A1. The V versus (V-I) colour-magnitude plot for data obtained by J95.

scattered all over the Cep OB3 region, with a field of view of just $3.0' \times 4.4'$ each. Therefore, for the first time, thanks to a wide surveyed area and deep photometry, we have been able to unambiguously detect a low-mass PMS population in the Cep OB3 association.

We cross-correlated our optical catalogue (just stars with zero-flags) with the J95 catalogue searching for correlations within an increasing radius. From the cumulative distribution of the number of matches obtained at different radii, the correlation radius at which we have obtained the maximum number of optical counterparts, before spurious correlations contributed significantly to the distribution, was found to be 1.85 arcsec (corresponding to 5 pixels on the CCD frames). Such big differences in positions are probably due to J95 astrometric errors, because our mean astrometric accuracy is about 0.4 arcsec. J95 used reference stars from the Guide Star Catalogue (GSC; with astrometric precision up to 0.8 arcsec; see Lasker et al. 1990), but they obtained an astrometric accuracy worse than 1 arcsec since the number of GSC reference stars falling on their fields is quite small. The limiting magnitude of the GSC in the Cep OB3 region is about $V=14$, therefore most of their fields contain just two reference stars.

We found more than 300 matches in total (within the correlation radius of 1.85 arcsec), for stars in fields 1a, 2a, 2b, and 4b. In Fig. A2 we compare our CCD measurements for V with the optical data given by J95, without restriction on the photometric errors: we find no systematic trend and a mean difference of about 0.04 mag. Analogously for (V-I), (B-V) and (U-B) colours we find mean differences of about 0.08, -0.04 and 0.06 respectively. The higher dispersion noticeable for fainter stars is an effect due in part to larger errors in the J95 catalogue, in part to some faint stars in our catalogue which are affected by light from a close saturated star, and thus have quite large photometric errors. However, note that in this paper we performed our analysis using an optical catalogue containing just good (i.e., with zero-flags) stars with photometric errors less than 0.1 mag. As an example, typical photometric errors in V, (B-V), (V-I) and (U-B) for stars in our catalogue at a given visual magnitude of $V=19$ for BVI colours and $V=17$ for (U-B) are respectively of 0.02, 0.05, 0.02 and 0.02.

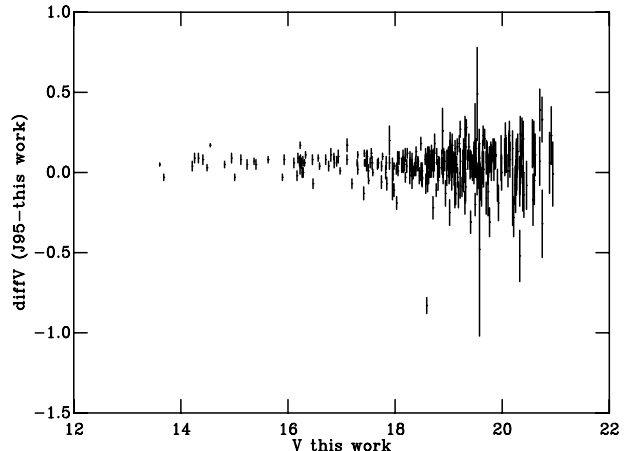


Figure A2. V magnitude differences J95 - this work versus visual magnitudes from this work for 302 matched stars. Error bars are the sum (in quadrature) of the errors for a given star from each catalogue.

APPENDIX B: ADDITIONAL EXTINCTION FOR THE BACKGROUND POPULATION

In Section 4 we have identified the objects plotted in the CMDs as belonging to a background sequence (the bluer) and a PMS (the redder), plus possible contamination from faint foreground stars. We noticed (see Fig. 3) that the background population in field 1a is also apparent as the blue sequence in each of fields 2a and 2b, whereas it is essentially absent from field 1b, positioned directly on the molecular cloud. In fields 3a, 3b, 4a and 4b (see Fig. 3), the background population of stars is still apparent but there is not the neat separation from the PMS population. Analogously, in Section 6, after isochrone fitting to the PMS objects, we noticed that in fields 1a and 2a there seems to be a neat separation between the two sequences (background and PMS): the 10-30 Myr gap is less populated. Instead in fields 2b and 3b we noticed no difference in the stellar densities moving from the 1 to 30 Myr isochrones. This can be explained by additional interstellar material in these directions, the background objects being shifted towards larger (V-I) colours, contaminating the 10-30 Myr gap and part of the PMS.

In fact, we found that it is possible to match the background populations of fields other than 1a (i.e., 2a, 2b, 3a, 3b, 4a and 4b; note that for field 1b no comparison is possible because it is looking at the cloud and most of the background sequence is missing) with that of field 1a, shifting them up and to the left (i.e., dereddening them), along the reddening vector. As an example, we have found that dereddening field 3a by an $A_V = 0.6 \pm 0.2$ brings the background sequence into agreement with that in field 1a (see Fig. B1). Analogously, it could be shown that the same argument holds for the other fields: in their CMDs, the background sequences match that in field 1a once they have been dereddened by an additional extinction value which is about $A_V = 0.15 \pm 0.10$, $A_V = 0.6 \pm 0.2$, $A_V = 0.5 \pm 0.2$, $A_V = 0.5 \pm 0.1$, $A_V = 0.8 \pm 0.2$ and $A_V = 1.4 \pm 0.2$ for fields 2a, 3a, 4a, 2b, 3b and 4b respectively.

Therefore, the majority of the stars filling the gap between the 10 and 30 Myr isochrones in all the fields other

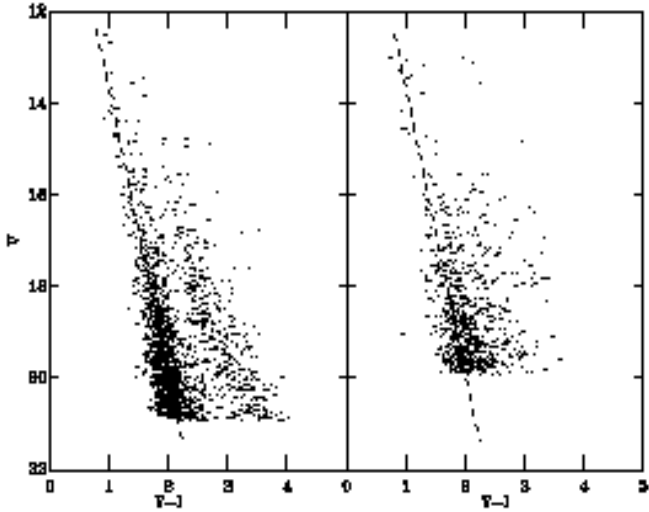


Figure B1. CMD of field 3a [right], dereddened by the additional $A_V = 0.6$ value (see text), necessary to match its background sequence with that of field 1a [left].

than 1a are background stars which are shifted towards redder colours. We think that this additional extinction is affecting just the background population and that it is due to different concentrations of interstellar material in the direction of these fields: as confirmed in Fig. 5, there is a considerable assemblage of stars beyond Cep OB3b and changing in the extinction values are perfectly plausible.

Whereas this is certainly true for fields 2a, 2b and especially 3a and 4a, which are farther away from the Cep OB3 molecular cloud (see Fig. 2), some doubts could be risen for 3b and 4b which are closer to the cloud: for these two fields, the molecular material could be responsible for most of the additional extinction we have determined. This also implies that we cannot rule out the presence of some heavily reddened (because they are more deeply embedded in the molecular material) PMS objects, but this would not alter the global appearance of the PMS locus in the CMDs of fields 3b and 4b.

This paper has been produced using the Royal Astronomical Society/Blackwell Science \LaTeX style file.